# Egyptian Journal of Chemistry

http://ejchem.journals.ekb.eg/

## Rose Bengal- Pioglitazone Drug Reaction Novel Products. Structures – Biological Activity and Cytotoxicity Relationship and Evaluation with Theoretical Calculations

**Mohamed A. Zayed[1]\*, Yasmeen S. Farrag[1], Mahmoud A. Noamaan[2]**
[1] *Chemistry Department, Faculty of Science, Cairo University, 12613- Giza, Egypt.*
[2] *Mathematics Department, Faculty of Science, Cairo University, 12613- Giza, Egypt.*

**T**HE PIOG-RBeng reaction novel products were characterized by thermal in comparison with spectroscopic data using FT-IR, ^{1}H-NMR, then confirmed by XRD measurements and Theoretical computational calculations. The software of Gaussian 09W package had been used for computations. The geometries of Rose bengal (RBeng), Pioglitazone (PIOG) drug and their reaction products were optimized using B3LYP method and (DFT)/GENECP level was obtained by using Def2TZVP basis set. The basis set 6-311++G (d, p) had been used for remainder atoms. The mixed basis set was used due to its flexibility. HOMO and LUMO energy values, chemical hardness and electronegativity had been calculated for compounds. NBO calculations were made for measurement qualitatively the intra-molecular delocalization in systems under investigation on the same level using (NBO 3.1) program implanted in Gaussian 09W. The theoretical calculations involved estimation of global reactivity descriptors, local descriptors and molecular electrostatic potential (MEP) maps. TD-DFT approximation was used to calculate the FT-IR and ^{1}HNMR spectra of the studied compounds; which actually compared with practical data. Successful correlation between experimental and theoretical calculations had been made to confirm structures of studied compounds. The X-ray diffraction (XRD) was used to study the crystallographic structures of compounds under investigation. The practical results are also correlated to theoretical calculations of electronegativity (X), polarizability, HOMO and LUMO values of PIOG and PIOG-RBeng reaction products. The vibrational frequencies were evaluated in comparison with the corresponding normal modes at the optimized geometry. The investigated compounds are highly effective against Hepatocellular carcinoma, Breast carcinoma and Colon carcinoma cells. It is concluded that; cancer cells over expression promotes tumorigenic functions; can be suppressed by reaction products inhibitors.

**Keywords**: Rose bengal reagent, Pioglitazone drug, Reaction products, Thermal and spectroscopic studies, Biological activities, Theoretical calculations.

## Introduction

Pioglitazone (PIOG) HCl possess the general formula $C_{19}H_{20}N_2O_3S.HCl$, (mol mass = 392.9 g mol$^{-1}$). It is a colorless prism from ethanol with a melting point of 193-194 °C. PIOG HCl has an IUPAC name 5-[[4-[2-(5-Ethyl-2 pyridinyl) ethoxy] phenyl] methyl]-2, 4-thiazolidinedione hydrochloride [1]. The geometrical structure and numbering system of the given drug are shown in Fig (1).

PIOG confirmed as an adjunct to improve glycemic control in adults with type 2 diabetes clinical settings [2] and as a stopper in horseracing [3].Lin et al, 2003 [4] developed LC/MS/MS method for simultaneous determination of PIOG and its two metabolites in human plasma.KumariKarra et al, 2012 [5] suggested another LC/MS/MS process for simultaneous determination of PIOG and Candesartan in human plasma using Irbesartan as an internal standard. Various HPTLC methods were also reported

using different plates and different mobile phases [6-8] for determination of PIOG in bulk and pharmaceutical dosage forms. These methods were simple and accurate.

M. Amanlou et al, 2010 [9]. Simple and extractive spectrophotometric method based on the formation of yellow ion-pair between the basic nitrogen of the drug and BCG in phthalate buffer of pH 2.4 for the determination of PIOG HCl in pure and pharmaceutical formulations. The ion-pair formed was extracted with chloroform and measured at 419 nm. M. Okdeh et al, 2014 [10] developed simple, extractive spectrophotometric method for determination of PIOG in pure form

and pharmaceutical formulations. This procedure based on the formation of ion-pair between PIOG and Chromotrope 2R in acidic buffer, giving purple color. UV-Vis spectrophotometric methods for determination of PIOG alone, or in a combination with other drug substances were reported [11-15]. Rose Bengal (RBeng) dye has the IUPAC name 4, 5, 6, 7-tetrachloro-2′, 4′, 5′, 7′-tetraiodofluorescein disodium salt (Acid Red 94) as given by Parham et al, 2011 [16]. It is an anionic water soluble xanthene dye as given by S.H. Mousavi et al, 2009 [17]; which first appeared in Schultz's tables in 1881 (Fig. 2) as mentioned by DanianXu and D. C. Neckers, 1987 [18].
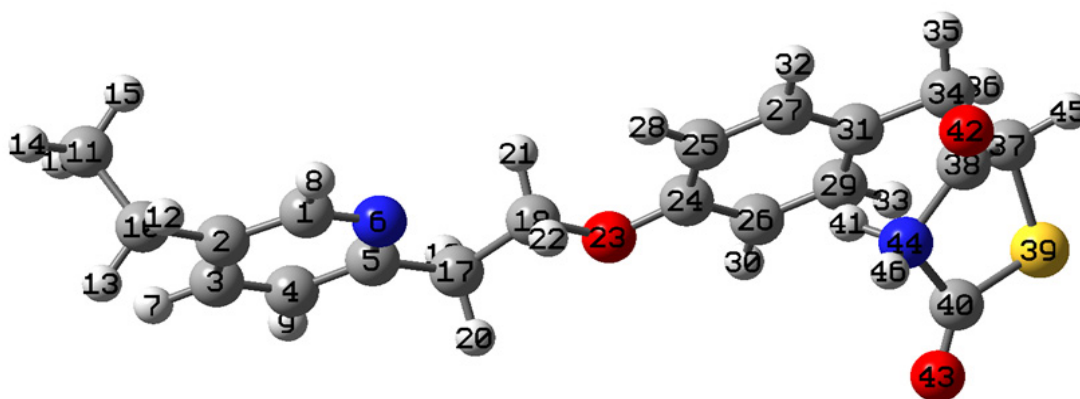


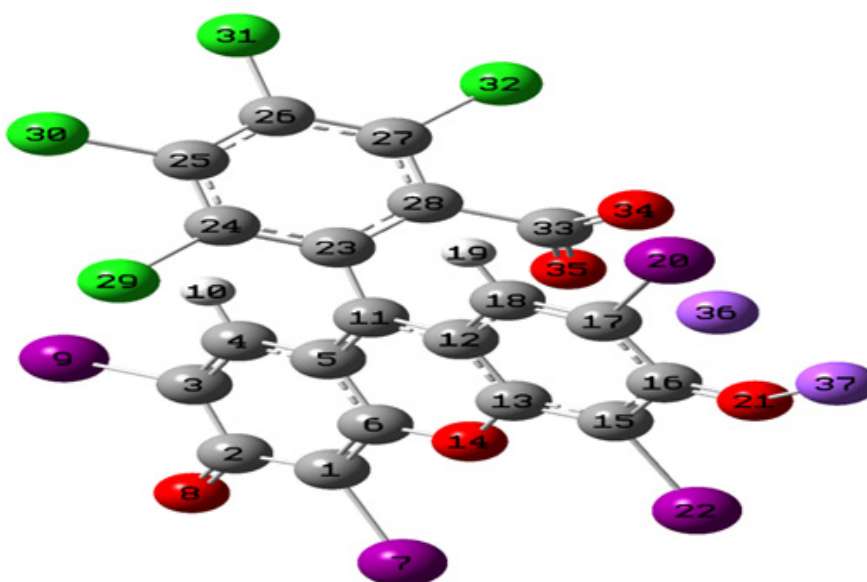**Fig. 1. The PIOG cation geometrical structure and numbering system.**



**Fig. 2. The structure and numbering system of RBeng.**

RBeng exhibits some unusual spectroscopic and photochemical properties. It has absorption coefficient in the visible region and a high tendency for inter-system crossing to produce a photochemically active triplet excited state due to its photo-activity [16]. RBeng had been used as a photodynamic sensitizer for cancer chemotherapy [19-22]. It also used as a topical ophthalmic diagnostic by Argueso et al, 2006 [23]. Wachter et al, 2003 [24] suggested it's for potential photodynamic therapy treatment of skin disorders without side effects in normal skin. Chang et al, 2008 [25] RBeng had been exploited as a promising sensitizer in wastewater treatment due to its water solubility, absorption in the visible region, good quantum yield of singlet oxygen, and inexpensiveness. RBeng Peptide conjugates were described by J.R. Carreon et al, 2005 [26] in featuring sequences that promote DNA binding. The complexation of these conjugates with DNA cause efficient quenching of the fluorophore singlet state and suppresses singlet oxygen production. The toxic character of RBeng (not as photosensitizer) against melanoma and as a promising chemotherapeutic agent in melanoma treatment had been reported by S. H. Mousavi et al, 2006 [27]. The direct cytotoxic and pro-apoptotic effects of RBeng on MCF-7 cells had been investigated [17] as a widely used model system for the study of breast cancer and also as human fetal skin fibroblasts (HFSF-PI3) as control non-malignant cell lines. RBeng was used by Joon Seok Lee et al, 2015 [28] to inhibit Alzheimer's β-amyloid (Aβ) aggregation. RBeng under green LED illumination exhibited a much stronger inhibition effect upon photo-excitation on Aβ aggregation than RBeng under dark conditions. Photo-excited RBeng suppressed the conformational transition of Aβ monomers into β-sheet-rich structures. Photo-excited RBeng is also used in the reduction of Aβ-induced cytotoxicity. Due to the toxicity level of the dye and its discharge into rivers from different laboratories, magnetic solid phase extraction (MSPE) based on cetyl-trimethyl ammonium bromide (CTAB)-coated magnetic iron oxide nanoparticles (C-MIONPs) was investigated [16].

Gaussian 09W software package was used for all computations [29]. The molecular structures of the studied compounds had been fully optimized using density functional theory B3LYP method. Where (B3) [30-32] stands for Becke's three parameters of correlation functions of Lee, Yang and Parr (LYP) [33]. DFT/GENECP level had been done by implementing Def2TZVP basis set for all atoms [34, 35]. On the other hand, 6-311++G(d,p) [36, 37] basis set had been used for the rest of atoms. During the geometry optimization no symmetry constrains were applied [38, 39]. Due to the flexibility, accuracy, consistent and better performance of the Alrich's effective core potentials basis set (def2-TZVP) with Gaussian type triple- $\zeta$ potential (6-311++G(d,p)) [40] we preferred to use this mixed basis set in our calculations. For compounds under test, the electronegativity and chemical hardness had been calculated using the following relations: X= (I + A)/2 (electronegativity), η=(I-A)/2 (chemical hardness), S = 1/2η (chemical softness) where I and A are ionization potential and electron affinity, and I= - EHOMO and A= - ELUMO, respectively [41,42,43].The NBO 3.1 program implemented in the Gaussian 09W software package had been used for NBO calculations at the same level. Using Chemcraft version 1.6 packages and Gauss View version 5.0.9 optimized structures were visualized throughout the whole of this work [45]. The first low-lying excited states for drug, reagent and their reaction products respectively had been calculated within the vertical linear-response TD-DFT approximation [45-50] at the same level of theory to calculate their theoretical FT-IR and $^1$HNMR spectra of thestudied compounds. The previously published equations [51-54] had been used for calculation of the total static dipole moment (μ), the mean polarizability <α>, the anisotropy of the polarizability and the mean first hyper-polarizability <β> using the x, y, z components.

## Experimental

### Materials and Reagents

The used chemicals included PIOG HCl (M.wt = 392.9 g mol$^{-1}$), that supplied by Elrazy Pharmaceutical Co, Ismailia (Egypt), also RBeng disodium salt reagent was supplied by BDH Chemicals Ltd, Poole, England. Absolute ethanol (99.8%, Sigma Aldrich, Germany), phosphoric acid (88 %, BDH, England), acetic acid (El Salam for chemical industries, Egypt), boric acid (ADWIC), Analar sodium hydroxide (Merck, Germany) were used. The distilled water, obtained from all glass equipment always used for solution preparation.

### Solutions

RBeng disodium salt (1 x 10$^{-3}$ M, M.wt = 1017.64 g mol$^{-1}$) had been prepared by dissolving weighed amount distilled water and the volume completed to 250 mL volumetric flask. PIOG

HCl solution of 1 x 10$^{-3}$ M (392.90 μg mL$^{-1}$) was prepared by dissolving 0.0393 g of the pure drug in 100 mL absolute ethanol.

### Preparation of the solid ion-pairs

The solid ion-pair of PIOG drug with RBeng had been prepared, by addition of a warm solution of RBeng (0.5088 g 0.5 mmol) in water; to warm solution of (0.1965 g, 0.5 mmol) PIOG dissolved in least amount of ethanol. The solid ion–pairs were obtained as a result of gentle warming of reaction mixture for 10 min. The obtained solid ion-pairs were filtered using a porcelain funnel and washed with warm water. These ion-pairs were dried and recrystallized from ethanol. The melting points of these ion-pairs were measured and recorded.

### Structure characterization of the solid drug and its solid ion-pairs with RBeng

The structures of the solid drugs and their ion-pairs were characterized and investigated by using elemental analyses (EA), spectroscopic tools (FT-IR, $^1$H-NMR and XRD). The data obtained were compared with theoretical calculations.

Elemental analyses (C, H and N) of solid products had been done using automatic CHN instrument (Elementar CHNS analyzer, model Vario EL III) at the Micro-analytical Center of Cairo University.

The infrared spectra of the solid drugs, solid reagent and their ion-pairs had been measured and compared with each other to know the groups shared in the formation of these solid ion-pairs. The wavenumbers of the characteristic peaks of corresponding groups at the drugs and the reagent were determined. Shifting of wavenumbers to lower or higher values referred to sharing of these groups in the formation of solid ion-pairs.

$^1$H-NMR analyses of different proton groups of the solid drugs, solid reagent and their ion–pairs were recorded and compared with each other. The chemical shifts of the different protons at the drugs and the reagent were determined. Changing of these chemical shifts, appearing and disappearing of the peaks referred to the places where the reactions took place.

### Instruments

Sensitive analytical balance of 0.0001g, RADWAG model As-220\c\1 (Poland) had been used for weights measurement. Magnetic stirrer theromostated hot plate (VELP-Europe) had been used for stirring and heating of reaction mixtures. The pH measurements were performed by HANNA pH-meter model pHS-3CW. The melting points of solid drugs and their ion–pairs had been performed using melting point apparatus of model Gallen Kamp, Germany.

The FT-IR spectra of solid compounds as KBr pellets were recorded using Jasco spectrophotometer model 4100 in wavenumber region 4000 – 400 cm$^{-1}$.

The Varian Mercury VX-300 NMR spectrometer used for $^1$H-NMR analyses. The $^1$H-NMR spectra were run at 300 MHz in dimethylsulphoxide (DMSO-d$_6$). Chemical shifts were quoted in δ and were related to that of the solvent.

### XRD measurements

The XRD data had been measured at Beni-Suef University using copper Cu Kα radiation (λ= 0.15406 nm) in the range of 5° to 80° at a scan rate (2θ) of 3°S-1) by the instrument, Analytical Expert Pro PW3040 MPD X-Ray Diffract meter XRD.

The XRD technique had been used to investigate the mineral components phases and crystallinity of the analyzed material for all samples. Kα Radiation was selected with a diffracted beam Monochromators to acquire X-ray patterns of enough intensity to detect the lines in angle 2θ of the mineral components of the samples.

### Main Graphics, Analyze View: (Bookmark 2)

XRD data configuration=Flat-Sample-Stage, Owner=User$^{-1}$, Goniometer=Theta/Theta; minimum step size 2 Theta: 0.0001; minimum step size Omega:0.0001, sample stage=Stage for flat samples/ holders, diffractometer system= EMPYREAN, measurement program=C:\ PANalytical\Data Collector\Programs\Nashaat 21.xrdmp, Identifier={A41C9BB2-B99B-4E5B-BD5D-74AA87F08027}

| Pos. [°2Th.] | Height [cts] | d-spacing [Å] | Rel. Int. [%] | Crystallite Size only [Å] | Micro Strain only [%] |
|---|---|---|---|---|---|
| 29.5968 | 13.26 | 3.01832 | 23.19 | 157.796400 | 0.956398 |
| 31.7657 | 57.16 | 2.81702 | 100.00 | 935.987000 | 0.150484 |
| 45.5218 | 26.05 | 1.99267 | 45.57 | 427.018500 | 0.233323 |

*Cytotoxicity*

The cytotoxicity of PIOG, RBeng and PIOG-RBeng product against Caco-2, Mcf7 and HepG2 cells had been detected in biological activity lab at El-Azhar University, using MTT practical protocol [55-57]. The 96 well tissue culture plates were inoculated with $1 \times 10^5$ cells / ml (100 µL / well) and incubated at 37°C for 24 hours to develop a complete monolayer sheet. Growth media were decanted from 96 well micro titer plates after confluent sheet of cells was formed. The cell monolayer was washed twice with suitable washing media. Two-fold dilutions of tested samples were made in RPMI medium with 2% serum (maintenance medium). 0.1 mL of each dilution was tested in different wells leaving 3 wells as control and receiving only maintenance medium. Plate was incubated at 37°C and examined. Cells were checked for any physical signs of toxicity, e.g. partial or complete loss of the monolayer, rounding, shrinkage, or cell granulation. MTT solutions had been prepared as 5mg/ml in PBS (BIO BASIC CANADA INC). 20 µL MTT solutions were added to each well; place on a shaking table of 150rpm for 5 minutes, to thoroughly mixing the MTT into the media. The mixture had been incubated at 37°C in 5% $CO_2$ for 1-5 hours to allow the MTT to be metabolized and finally the medium dumped off. The dried plate on paper towels had been used to remove residue if necessary. Formazan MTT metabolic product had been suspend in 200 µL DMSO. The mixture placed on a shaking table (150 rpm for 5 minutes) to thoroughly mix the formazan into the solvent. The optical density recorded at 560 nm and subtracts background at 620 nm and the optical density directly correlated with cell quantity.

## Results and Discussion

*Structure characterization of PIOG-RBeng product*

The structure of PIOG-RBeng separated solid product had been identified using different techniques such as elemental analyses (C, H, and N); UV-Vis spectra, FT-IR, ^{1}H-NMR and its crystallinity had been checked by X-ray diffraction (XRD). The products spectra were compared with those of the PIOG drug and RBeng reagent during structure investigation.

*Electronic absorption spectra*

*Maximum Wavelength ($\lambda_{max}$) of RBeng reagent and its reaction product with PIOG*

The aqueous solution of RBeng reagent (gives red color) and its reaction product with PIOG (gives pink color) were scanned separately against distilled water and RBeng solution as a blank, respectively, in the wavelength range 450–650 nm, as given in Fig (3.a, b).
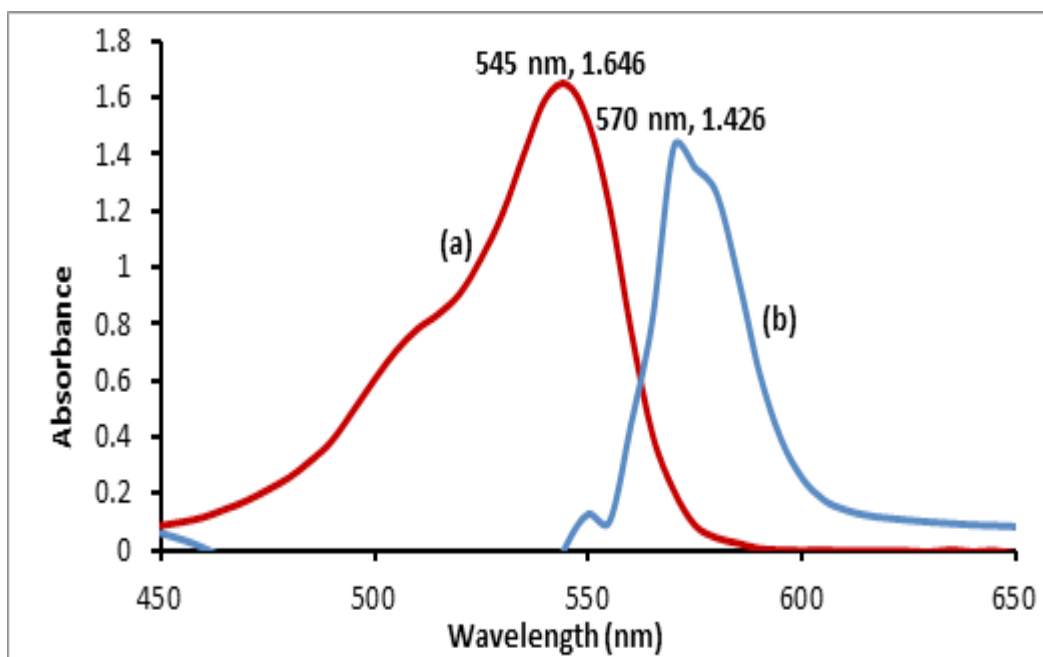


**Fig. 3. Vis. absorption spectra of   (a) RBeng 0.25 x 10^-4 M., (b) PIOG (10^-4 M) - RBeng (10^-4 M) reaction product.**

The obtained absorption spectra of the formed product are shown in Fig (3b). It gives maximum absorption at $\lambda_{max}$ = 570 nm of molar absorptivity $\varepsilon$ = 1.426 x $10^4$ L mol$^{-1}$ cm$^{-1}$. It may be due to $\pi$–$\pi^*$ transition in the phenyl rings as illustrated from the FMOs. These data indicate that the $\lambda_{max}$ of the product red shifted to higher wavelength far from that of RBeng at $\lambda_{max}$545 nm; which might originate from n–$\pi^*$ affected by $\pi$–$\pi^*$ transition. This may be attributed the strong interaction between RBeng anion and drug cation to give ion-pair product. The molecular orbital calculation indicates that these maxima are mainly originated from the $\pi$–$\pi^*$ transition in the PIOG $\pi$–system with good contribution from RBeng molecular orbitals. These results also enforce that there are good charge–transfer and H-bonding interactions between drug and reagent. The TD–DFT calculation results of the gaseous state show moderate agreement with the experimental ones.

*Elemental Analyses of solid product (1:2, R:D)*

The elemental analyses results, analytical and physical data of PIOG-RBeng product (1:2, R: D) is given in Table 1.

The data obtained confirm the formation of RBeng-Drug ion pair in ratio 1:2 (R: D) of high m.p.= 180 ℃ referring to the thermal stability of this ion-pair.

*FT - IR analysis*

Both practical and theoretical FT-IR spectral data of RBeng, PIOG and their ion-pair product are shown in Fig (4).

**TABLE 1. Analytical and physical data of PIOG-RBeng product.**

| The Product | Color | R : D | m. p (℃) | Elemental analysis Found (calcd %) | | |
| --- | --- | --- | --- | --- | --- | --- |
| | | | | C | H | N |
| PIOG – RBeng ($C_{58}H_{42}Cl_4I_4N_4O_{11}S_2$) Mol Mass = 1685.46 | Red | 1 : 2 | 180 | 41.8 (42.32) | 2.15 (2.51) | 3.09 (3.33) |

RBeng reagent (R) ($C_{20}H_2Cl_4I_4O_5$, mol mass = 971.66 g mol$^{-1}$), PIOG drug (D) ($C_{19}H_{20}N_2O_3S$, mol mass = 356.9 g mol$^{-1}$).
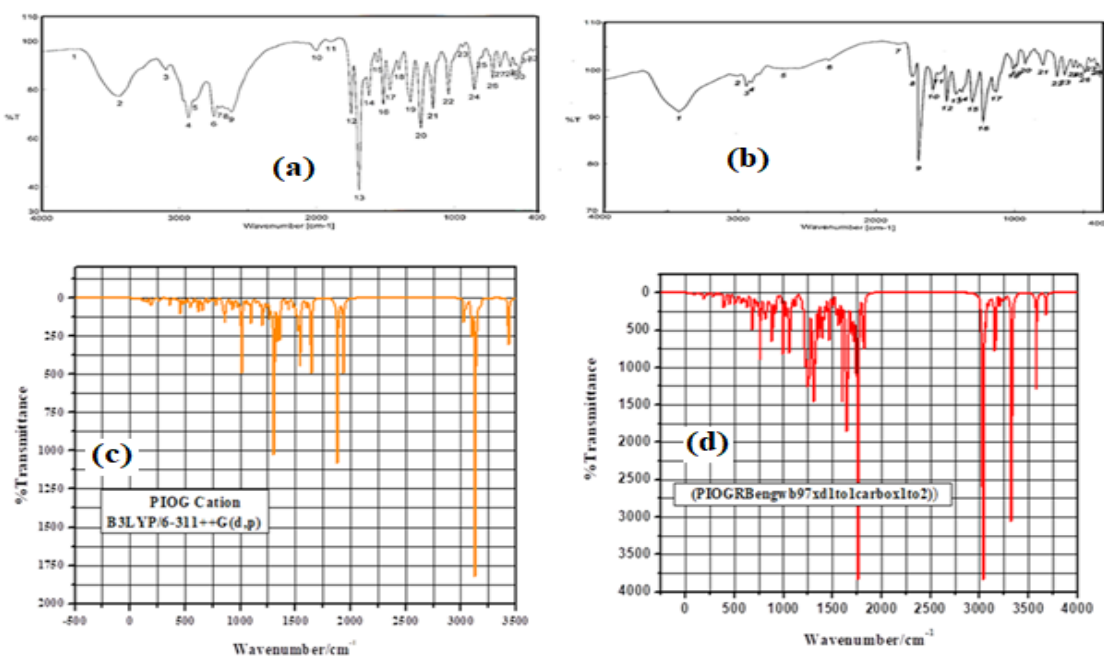


**Fig. 4. (a) Practical FT-IR spectra of PIOG, (b) Practical FT-IR of PIOG-RBeng reaction product, (c)Theoretical FT-IR spectra of PIOG, (d) Theoretical FT-IR of PIOG-RBeng reaction product.**

From these figures some selected importance vibrations of the given compounds are identified and are listed in Table 2.

From Figure (4) and tabulated data (Table 2); the FT-IR of RBeng refers to the bands of $\nu$ (C= O) stretching of the carboxylate at 1550.49 and 1492.63 cm$^{-1}$(Theoretical at 1400-1500 cm$^{-1}$). These bands are shifted to lower values of wavenumbers, 1540.85-1511.92 cm$^{-1}$ and 1490.7-1447.31 cm$^{-1}$(Theoretical at 1400- 1575 cm$^{-1}$) in spectrum of PIOG-RBeng product [57]. The FT-IR of PIOG refers to the bands of $\nu$(C-H) stretching of the aliphatic alkane at 2742.28 and 2615.97 cm$^{-1}$(Theoretical at 2900-3100 cm$^{-1}$), $\nu$ (C= O) stretching of the amide at 1742.37 and 1690.3 cm$^{-1}$( Theoretical at 1750-1780 cm$^{-1}$) [57]. These bands are shifted to higher values of wavenumber in the corresponding PIOG–RBeng product at 1760.69 (theoretical at 1775-1780 cm$^{-1}$) and 1701.87 cm$^{-1}$(Theoretical 1700 cm$^{-1}$) and $\nu$(C-H) stretching bands of the aliphatic alkane at 2742 and 2615 cm$^{-1}$are disappeared in the spectrum of ion-pair product. The shift of the bands frequencies of some groups of RBeng and PIOG into lower and/ or higher wavenumbers may be attributed to the electrostatic attraction and/or hydrogen bonding between the cationic drug and the anionic form of RBeng reagent during the formation of their ion-pair product. The observed shift of the carbonyl band of RBeng may indicate the involvement of its carbonyl oxygen atom in some sort of molecular interactions due to formation of hydrogen bonds as confirmed by theoretical calculations.

The theoretically calculated and found FT-IR bands were found to be in good agreement. From the above results, it is clear that the interaction between the studied molecules proceeds through proton–transfer followed by ion–pair formation with the formation of several hydrogen bonds which gives the resulting product of an extra stability.

*¹H-NMR analysis*

The ¹H-NMR spectral data of RBeng, PIOG and their reaction product are shown in Fig (5).

From Figure 5 some selected ¹H-NMR protons chemical shifts of the given compounds are identified (Table 3).

From data obtained in (Fig. 5 and Table 3); the ¹H–NMR spectrum of RBeng; shows two peaks of chemical shifts 7.410 and 7.912 ppm; which correspond to the protons of aromatic rings. These peaks re-appear in the ¹H–NMR spectrum of PIOG-RBeng product at 8.420, 7.500 ppm; which refers to the presence of RBeng in this product. the ¹H–NMR spectrum of PIOG; shows peak at 12.008 ppm; which corresponds to the proton of NH, peaks at range 8.698-7.902 ppm; which corresponds to the protons of pyridine ring (C1, C3 and C4), peaks at the range 7.159-6.858 ppm; which corresponds to the aromatic ring (C25-29). The methine proton (C37) shows peaks with chemical shifts 4.861-4.837 ppm [58]. The spectrum also shows peaks corresponds to the methylene groups (C34, C17, C18 and C10) protons in the range of 4.414-2.438 ppm and peaks corresponds to the methyl group (C11) at 1.255-1.204 ppm [58]. These peaks are shifted in the ¹H–NMR spectrum of PIOG-RBeng product to 12.100 ppm for NH proton, 7.713-7.368 ppm for the pyridine ring protons, 7.148-6.843 ppm for the aromatic ring (C25-29) protons, 4.327-4.284 ppm for the methine (C37) proton, 4.327-1.908 ppm for the methylene groups (C34, C17, C18 and C10) protons and to 1.210-1.057 ppm for the methyl group (C11) protons. These changes in chemical shifts may be due to the electrostatic attraction between the cationic drug and the bulky anionic reagent (small charge/unit volume).

**TABLE 2. FT- IR characteristic peaks of the PIOG, RBeng and their reaction product.**

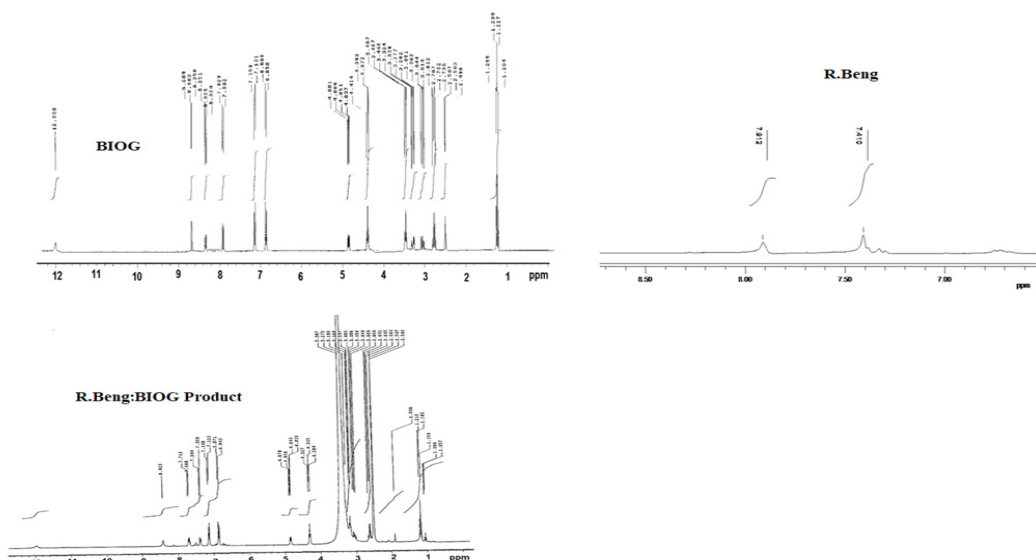| Compound | $\nu$ C-H stretching of aliphatic alkane | $\nu$ C= O stretching of the amide | $\nu$ C= O stretching of carboxylate | $\nu$ C-O Stretching of carboxylate |
|---|---|---|---|---|
| **Rbeng reagent** | - | - | 1550.49 and 1492.63 | 950.734 |
| **PIOG drug** | 2742.28 and 2615.97 | 1742.37 and 1690.3 | - | - |
| **P I O G - R B e n g Product** | disappeared | 1760.69 and 1701.87 | 1511.92 and 1447.31 | 1041.37 |

**Fig. 5.** The ¹H-NMR spectral data of RBeng, PIOG and their reaction product.

**TABLE 3.** ¹H-NMR spectral data of RBeng, PIOG and their reaction product.

| Compound | δ H of NH (ppm) | δ H of C1, C3 and C4 of the pyridine ring (ppm) | δ H of aromatic rings (RBeng Part) (ppm) | δ H of C25,26,27,29 (ppm) | δ H of C37 (ppm) | δ H of C17, C18 (ppm) | δ H of C34 (ppm) | δ H of C10 (ppm) | δ H of C11 (ppm) |
|---|---|---|---|---|---|---|---|---|---|
| PIOG | 12.008 | 8.698-7.902 | - | 7.159-6.858 | 4.861-4.837 | 4.414-3.324 | 3.309-3.014 | 2.812-2.438 | 1.255-1.204 |
| PIOG-RBeng Prod. | 12.100 | 7.713-7.368 | 8.420, 7.500 | 7.148-6.843 | 4.327-4.284 | 4.327-3.275 | 3.190-3.009 | 2.656-1.908 | 1.210-1.057 |
| RBeng | - | - | 7.410, 7.912 | - | - | - | - | - | - |

*Thermal analyses*

Thermograms of RBeng, PIOG and their reaction product are shown in Fig. 6.

The TG curve of RBeng (Fig. 6.a) refers to its decomposition in three steps of total estimated mass loss of 98.61% (calcd. 97.27%). The first step occurs at 35-214 °C of estimated mass loss of 11.14% (calcd. 10.46%); which may be related to the loss of 3Clradicals. This process is accompanied with a small exothermic peak according to the DTA (Fig. 6.a) at temperature 114.1 °C; this exothermic peak may be attributed the chemical recombination of chlorine radicals to form chlorine volatile molecules. The second step

occurs at 215-671 °C of estimated mass loss of 63.55% (calcd. 63.82%); which may be related to the loss of $Na_2CO_3$, $2I_2$ and Cl radical. This loss is confirmed by the appearance of exothermic peak in DTA at temperature 522.4 °C; which related to chemical recombination of halogen radicals to form volatile halogen gases. The third step occurs at 671-954 °C of estimated mass loss of 23.92% (calcd. 22.99%); which may be related to the loss of $C_{18}H_2O$ and CO gas. This process appears as endothermic peak in DTA at temperature 821.08 °C. Therefore, these thermal decomposition peaks of RBeng are presented by the proposed scheme (1).
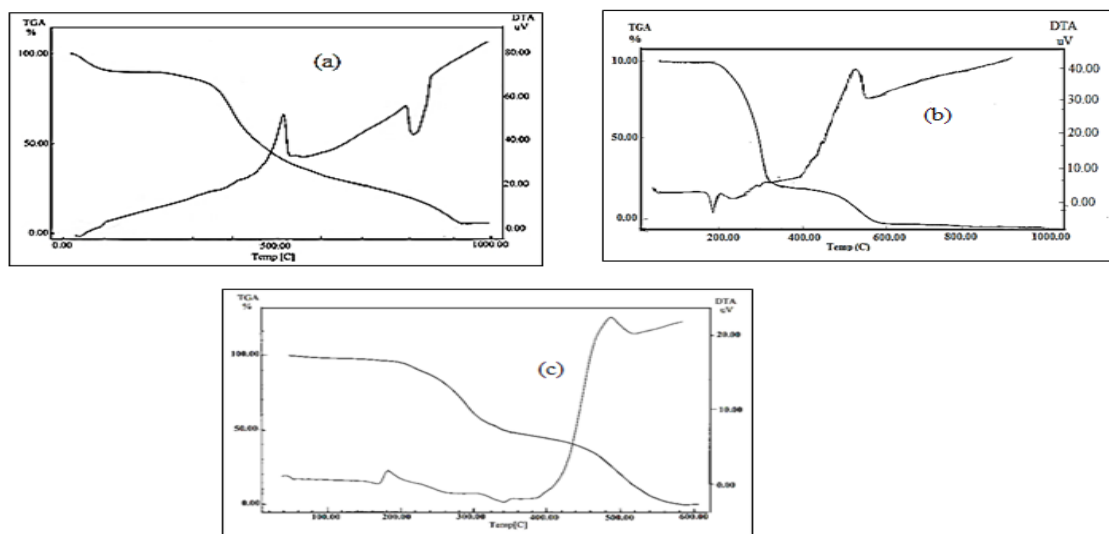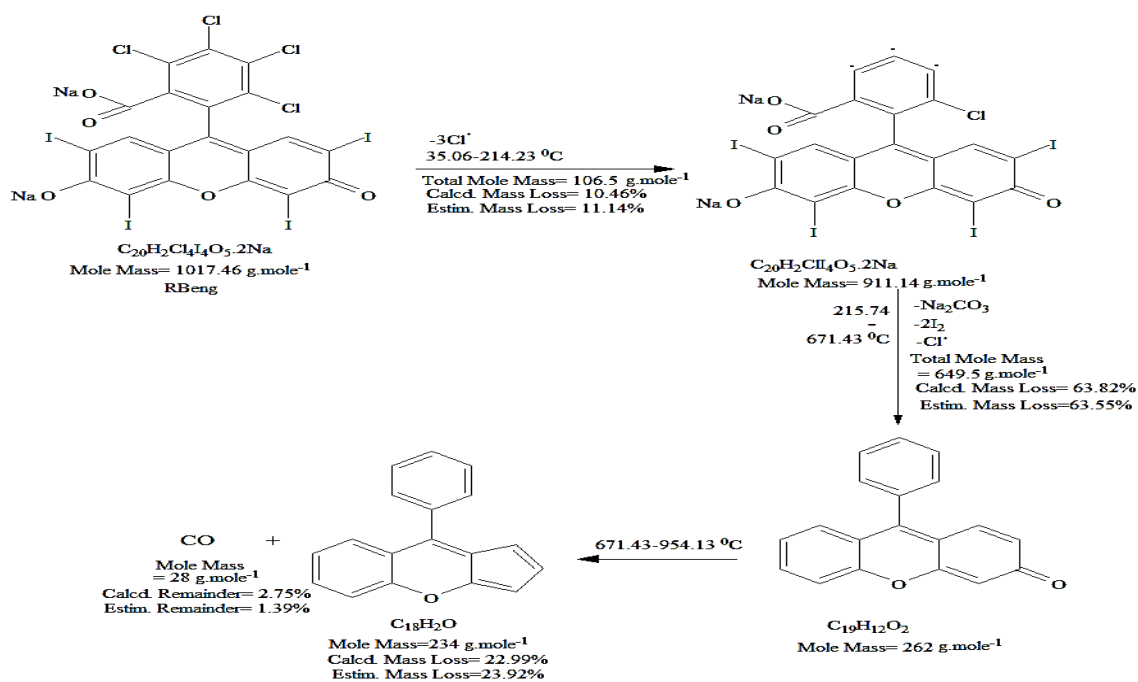
**Fig. 6. TGA-DTA curves of (a) RBeng, (b) PIOG HCl, (c) PIOG-RBeng product.**



**Scheme 1. The proposed thermal decomposition scheme of RBeng**

The TGA of PIOG (Fig. 6.b) shows that, it decomposes in two main steps with total estimated mass loss of 95.24 % (Calcd % = 96.72%). The first step occurs at 68-334 °C; this may be related to the loss of $CH_3$ and $C_{12}H_{12}NO_3S.HCl$ radicals (Estim. % = 75.53 %, Calcd. % = 76.61 %). This step is confirmed by the appearance of endothermic peak in DTA (Fig. 6.b) at 299.0 °C. The second step

at 410–600 °C; may be attributed to the loss of pyridine molecule $C_5H_5N$ (Estim. % = 19.71 % and Calcd. % = 20.11 %) leaving $CH_2$ as a final residual. This appears at DTA as a very strong exothermic peak at 533.0 °C; which may be related to the loss of HCl gas and chemical rearrangement of $CH_2$ to $C_2H_4$ volatile gas. The thermal decomposition scheme of PIOG can be represented at Scheme (2).

The TGA of PIOG-RBeng ion-pair (Fig. 6.c) refers to its thermal decomposition in two steps with total estimated mass loss of 98.40% (Calcd. % = 99.67%). The first step at 40-309 °C; may be due to the breaking of the ion-pair and the loss of 2PIOG molecules (Estim. % = 43.36%, Calcd. % = 42.36%). This process is accompanied with exothermic peak according to DTA (Fig. 6.c) at 178.4°C. The second step at 309-584 °C with Estimated mass loss = 55.04% (Calcd. % = 57.28%). This step is accompanied by two peaks at the DTA, small endothermic peak at 341.6 °C followed by strong exothermic one at 497.7 °C, so this step may occurs at two stages. The first stage may be the loss of $2I_2$ and $2Cl_2$ and the second one may be the loss of $C_{19}H_{12}O_2$, $CO_2$ and $H_2O$ as a final step. The thermal decomposition scheme of PIOG-RBeng product can be represented at Scheme (3).



**Scheme 2. Thermal decomposition pathway of PIOG HCl.**



**Scheme 3.Thermal decomposition pathway of PIOG-RBeng product.**
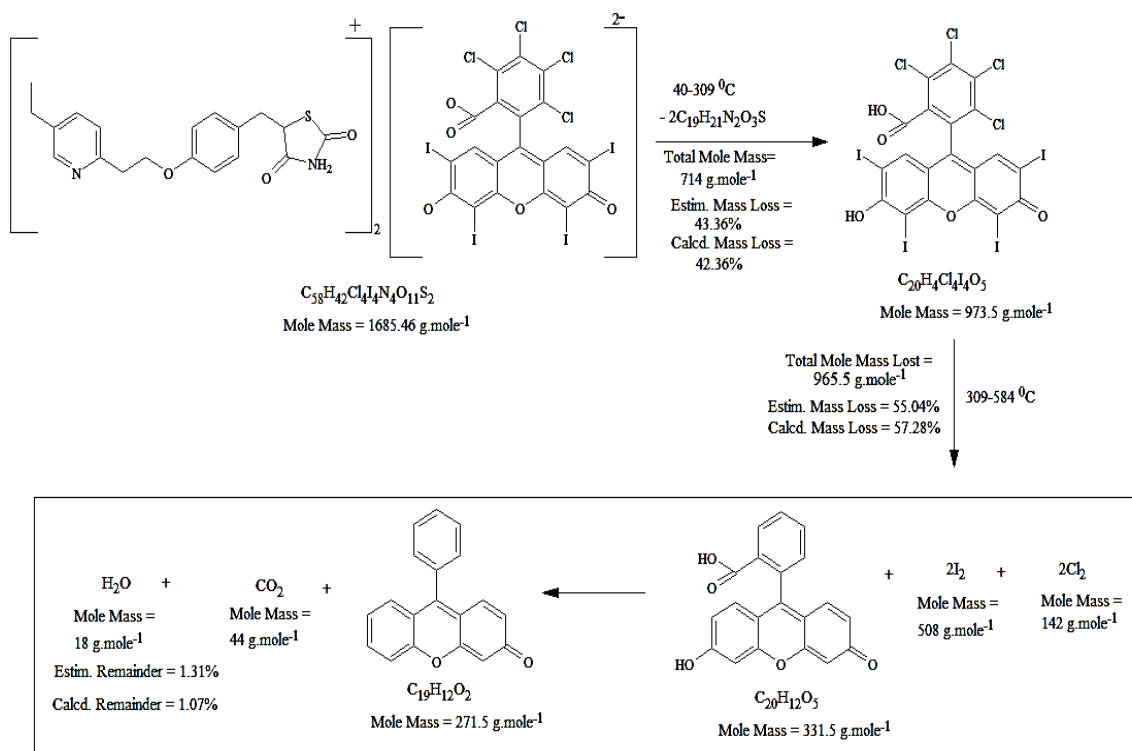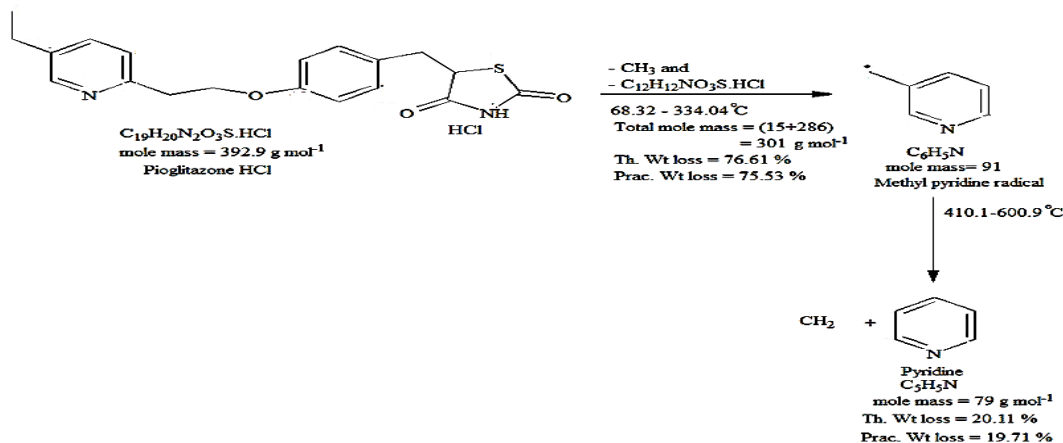
*XRD data and discussion*

*The XRD graphs of RBeng anionic reagent, PIOG drug cation and their reaction product (1:2) are given in Figure (7)*

The crystallographic data of the compounds are given in Tables 4-6.

From Fig 7 and Table 4; the XRD data of RBeng reagent refer to the presence of two crystalline peaks at 2θ[°2Th.] = 8.77 and 28.21 of heights 6.67 and 18.9 [cts], of d-spacing 10.07 and 3.16 °A, Rel. Int. [%] of 35.29 and 100%, crystalline sizes of 220 and 264 °A. Most of other peaks may refer to less crystalline sizes of the remainder part of the RBeng.

XRD data and Graphs of PIOG drug are shown in Table 5.

Table 5 and Fig 7 show the XRD data of PIOG drug. These data refer to crystalline structure of the drug and it has three clear lines. These lines have the data of Pos. [°2Th.] of 29.59, 31.76 and 45.52 of heights 13.26, 57.16 and 26.05 [cts]. It also have d-spacing [Å] of 3.018, 2.817 and 1.993 [Å] of Rel. Int. = 2.19, 100 and 45.57 [%] respectively. These three peaks refer to crystalline sizes of 157.79, 935.98 and 427.018 [Å] respectively.

XRD of RBeng-PIOG product (1:2, S4) data are shown in Table 6.

The crystallographic results of the (1:2) product (Fig 7 and Table 6) data refer to the appearance of two lines of Pos. [°2Th.] of 5.60 and 14.24, Heights 6.62 and 8.80 [cts], d-spacing of 15.77 and 6.26 [Å], Rel. Int. of 75.25 and 100.00 %, crystalline sizes of 63.34 and 153.79 [Å] respectively.

Comparing XRD data of ion-pair product with that of RBebg (R) and PIOG drug refer to complete shift of the two lines of the product Pos. [°2Th.] of 5.60 and 14.24 from that of Rbeng [°2Th.] = 8.77 and 28.21 of heights 6.67 and 18.9 [cts] and of drug three lines of Pos. [°2Th.] of 29.59, 31.76 and 45.52 of heights 13.26, 57.16 and 26.05 [cts]. The complete change in crystallinity of the product refers to the new physical nature of this product different from that of reactants. This conclusion is confirmed by the changes in another XRD data such as Rel. Int. of 75.25 and 100.00 %, crystalline sizes of 63.34 and 153.79 [Å] of the product from that of reagent Rel. Int. [%] of 35.29 and 100%, crystalline sizes of 220 and 264 °A and of drug d-spacing [Å] of 3.018, 2.817 and 1.993 [Å] of Rel. Int. = 2.19, 100 and 45.57 [%] respectively.
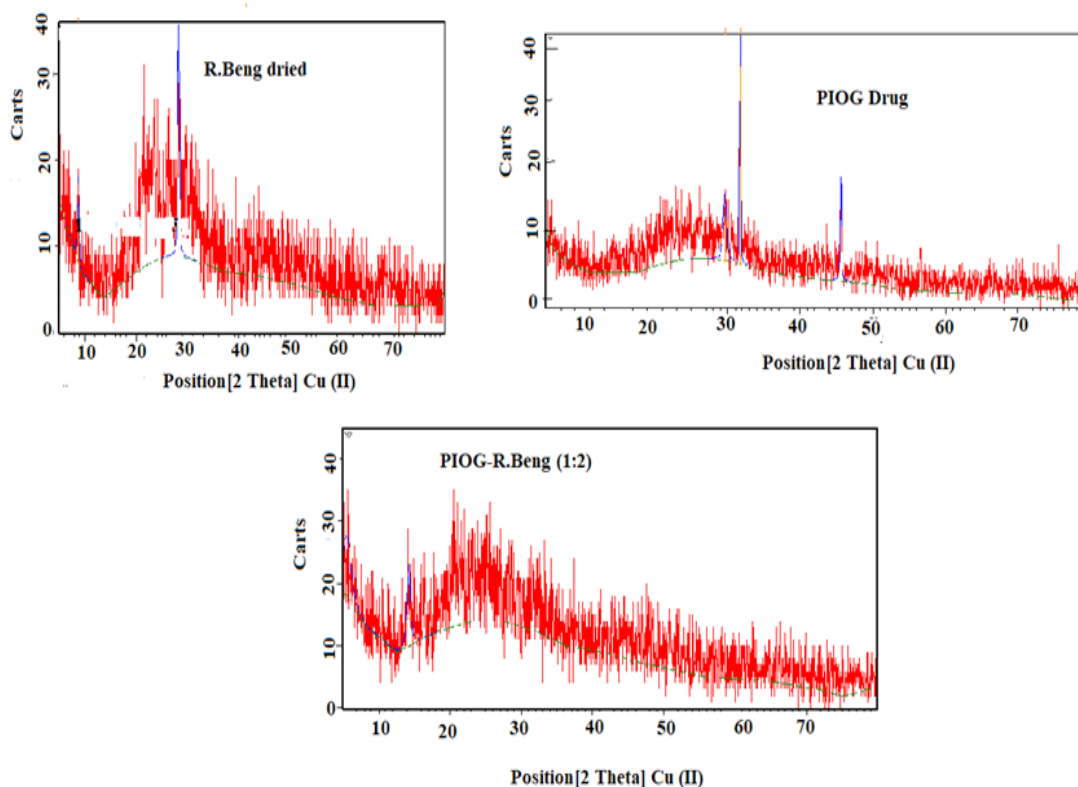


**Fig. 7. XRD graphs of RBeng (S1), PIOG (S2)and 1:2 reaction product dried sample (S4).**

**TABLE 4. Main Graphics, Analyze View of RBeng Dried sample (S2).**

| Pos. [°2Th.] | Height [cts] | d-spacing [Å] | Rel. Int. [%] | Crystallite Size only [Å] | Micro Strain only [%] |
|---|---|---|---|---|---|
| 8.7768 | 6.67 | 10.07535 | 35.29 | 220.145300 | 2.288341 |
| 28.2136 | 18.91 | 3.16307 | 100.00 | 264.981000 | 0.596849 |

**TABLE 5. Main Graphics, Analyze View of PIOG drug (S1).**

| Pos. [°2Th.] | Height [cts] | d-spacing [Å] | Rel. Int. [%] | Crystallite Size only [Å] | Micro Strain only [%] |
|---|---|---|---|---|---|
| 29.5968 | 13.26 | 3.01832 | 23.19 | 157.796400 | 0.956398 |
| 31.7657 | 57.16 | 2.81702 | 100.00 | 935.987000 | 0.150484 |
| 45.5218 | 26.05 | 1.99267 | 45.57 | 427.018500 | 0.233323 |

**TABLE 6. The Main Graphics, Analyze View of 1:2 product (S4).**

| Pos. [°2Th.] | Height [cts] | d-spacing [Å] | Rel. Int. [%] | Crystallite Size only [Å] | Micro Strain only [%] |
|---|---|---|---|---|---|
| 5.6026 | 6.62 | 15.77447 | 75.25 | 63.341880 | 12.451850 |
| 14.2419 | 8.80 | 6.21904 | 100.00 | 153.792500 | 2.021891 |

*Theoretical Calculations*

In theoretical calculations of the interaction between PIOG drug cationic molecule (S1) and the bulky anionic RBeng reagent (S2) seems at first trial is difficult. Therefore it is tested through first trial and considers the reaction goes as 1:1 ratio to give RBeng-PIOG product (S3). After successful first trial it is followed by second trial to give final 1: 2 product (S4) that previously separated and structurally studied in solid state. The calculations involved estimation of global reactivity descriptors, local descriptors and molecular electrostatic potential (MEP) maps.

*Molecule orbital calculations (DFT)*
 *Geometry optimization*
The fully optimized geometry of PIOG (S1) drug and Rbeng reagent (S2) are shown in Fig. 8.

The pyridine and phenyl rings of PIOG are in one plane and phenyl group attached with thiazole ring through CH2 that make an angle of about 112.46° with each other. The thiazole ring with the two hydrogen atoms on N1 atom; the H45–N40 and H46–N40 bond lengths are 1.042 and 1.027 Å respectively. The ethyl group is attached to pyridine ring in C3 position. The dipole moment of PIOG is 11.92 Debye. The molecule belongs to C1 symmetry point group. On the other hand, RBeng reagent (S2) is composed of three fused rings in one plane attached to another substituted phenyl ring out of plane through a carbon atom C11. The carboxylic group appears at C28 and another oxy group appears at C2 which bear two negative charges. RBeng belongs to C1 symmetry point group and it has a dipole moment of 8.26 Debye. The energy gap for RBeng is smaller than that of PIOG; which indicates higher reactivity and ability for light absorption in the visible region by RBeng.

*Frontier molecular orbitals (FMOs) analysis and Global Descriptors*

The calculated global reactivity descriptors included HOMO, LUMO, energy gap ($\Delta E_{gap}$), chemical hardness (η, eV), electronegativity (χ, eV), chemical potential (μ, eV), electron affinity (A), ionization potential (I), chemical softness(S), total energy (ET, au), Binding energy, and Nueclophilicity Index (N) . The results of the calculated parameters are given in Table 7.

The data in Table 7 show that; the values of RBeng reagent refer to its high reactivity and it is more soft ( S = 0.17, eV), less hard (η = 2.99), low electronegativity (χ = -0.83), low chemical potential (μ = 0.83), and of low electrophilicity (ω = 0.11), electron affinity (A = -3.81), and consequently attracted to cationic drug molecule. These data also refer to that; cationic drug

molecule is more hard ($\eta$ = 3.12), less soft ( S= 0.16), of more electron affinity (A =4.47), high electronegativity ($\chi$ = 7.66), of very low chemical potential ($\mu$ = -7.59) and of high electrophilicity ($\omega$ = 9.22). This electrostatic interaction between soft active reagent and hard cationic drug leads to the formation of 1:1 (R:D) of total energy (HT = -4495.24 kJ mol$^{-1}$) of dipole moment (14.64 Debye)and the more stable product (1:2, R:D)

of total energy ( HT = -5964.99 kJ mol$^{-1}$) and of dipole moment (4.23 Debye) in comparison with reactants. This conclusion is confirmed by the energy gap data between E$_{HOMO}$, E$_{LUMO}$ obtained from frontier molecular orbital (FMO) energies of the studied compounds that calculated using B3LYP/GENECP presented in Fig. 8 and molecular orbitals of reactants and resultants in Fig. 9.
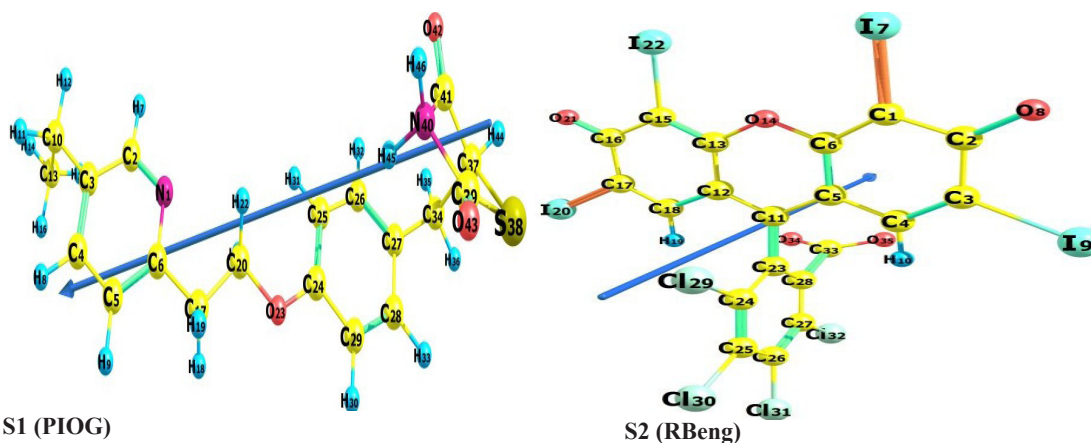


**S1 (PIOG)**                **S2 (RBeng)**

**Fig. 8. The optimized geometry, numbering system, vector of dipole moment of RBeng and PIOG compounds using WB97XD/GENECP level of calculation.**

**TABLE 7. Quantum chemical parameters Global reactivity descriptors of RBeng, PIOG drug and their reaction products using B3LYP/GENECP level of theory of the studied molecules (S1-S4).**

| Parameters | PIOG (S1) | RBeng (S2) | PIOG-RBeng (S3) | PIOG-RBeng- PIOG (S3) |
|---|---|---|---|---|
| ET,au | -1469.48314 | -3025.46530 | -4495.24498 | -5964.99567 |
| Binding Energy, | | | -185.59 | -353.03 |
| E(HOMO) | -10.71 | -2.16 | -5.75 | -8.03 |
| E(LUMO) | -4.47 | 3.81 | 0.67 | -0.72 |
| Energy gap, $\Delta$E eV | 6.24 | 5.97 | 6.42 | 7.32 |
| Ionization Potential, $I$ (eV) | 10.71 | 2.16 | 5.75 | 8.03 |
| Electron Affinity, $A$ (eV) | 4.47 | -3.81 | -0.67 | 0.72 |
| Dipole moment Debye | 11.92 | 8.26 | 14.64 | 4.23 |
| Chemical hardness, $\eta$ (eV) | 3.12 | 2.99 | 3.21 | 3.66 |
| Chemical potential, $\mu$ (eV) | -7.59 | 0.83 | -2.54 | -4.37 |
| Electrophilicity Index, $\omega$ (eV) | 9.22 | 0.11 | 1.01 | 2.62 |
| Electronegativity, $\chi$, eV | 7.59 | -0.83 | 2.54 | 4.37 |
| Global softness, S, eV | 0.16 | 0.17 | 0.16 | 0.14 |
| Nueclophilicity Index N, eV | -6.5 | 2.05 | -1.54 | -3.82 |

I =IP= - E$_{HOMO}$, A =EA = - E$_{LUMO}$, Electronegativity ($\chi$) = (I+A)/2, Hardness ($\eta$) = (I-A)/2, Softness (S) = 1/ $\eta$ Chemical potential ($\mu$) = - (I+A)/2, Electrophilicity ($\omega$) = $\mu^2$/ 2 $\eta$
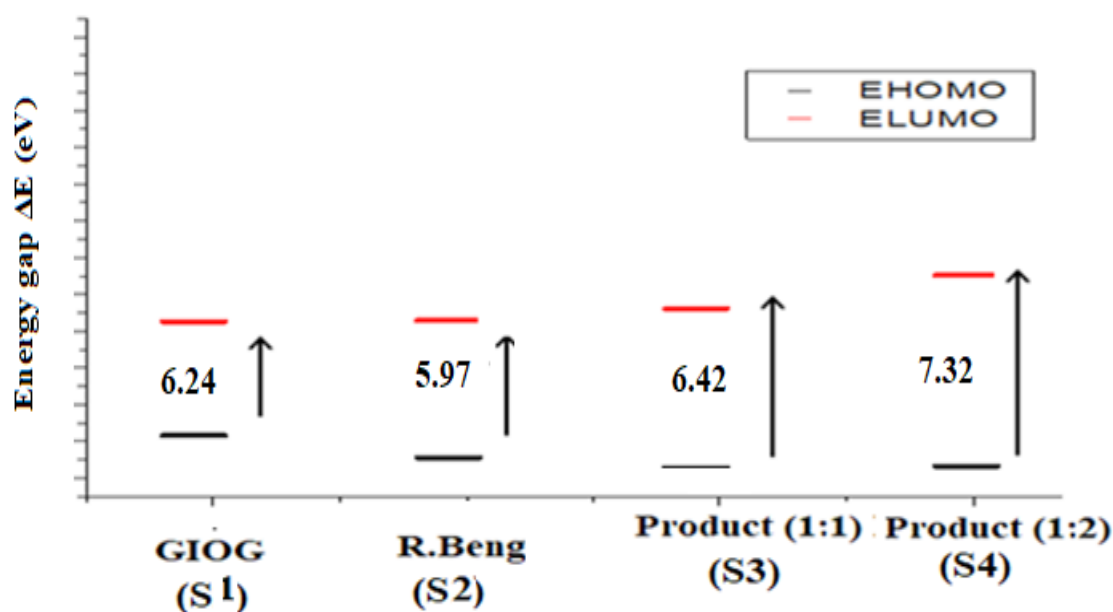
**Fig. 9. Relation between E$_{HOMO}$, E$_{LUMO}$ and E$_{gap}$ of PIOG (S1), RBeng (S2), RBeng-PIOG (S3,1:1) and RBeng-PIOG (1:2, S4) using B3LYP/GENECP level of theory.**

FMOs analysis is mainly required for studying electronic transitions and excited states of molecules. E$_{HOMO}$ indicates the ability to donate electrons while E$_{LUMO}$ indicates the ability to accept electrons during electronic transitions. The definition for ionization energy (I) and electron affinity (A) based on the HOMO–LUMO energy gap as I = −E$_{HOMO}$ and A = −E$_{LUMO}$; were involved in Koopman's theorem [21-22, 31].

Softness (S) had been computed as the half of reciprocal of hardness (η) and η = (I − A)/2; while the chemical potential (μ) and electronegativity (χ) can was calculated from FMOs analysis as follows: μ = −(I + A)/2 and χ = (I + A)/2 [24]. The electrophilicity index (ω) was measured the energy lowering resulting from maximal electron flow between donor and acceptor. It is calculated as ω = μ²/2η [33]. These descriptors are important to explain the reactivity and stability of compounds.

The obtained chemical potential values for PIOG and RBeng are −7.59 and 0.83 eV respectively. PIOG (ω = 9.22 eV) acts as a center for nucleophilic attack because it has a higher electrophilicity index than RBeng (ω = 0.11 eV). FMOs of the product (S3) of 1:1 PIOG-RBeng shows no charge–transfer

from one of the molecules to the other. This phenomenon is mainly attributed to the fact that; because both HOMO and LUMO originate from RBeng which supports the hypothesis of ion–pair formation after the proton–transfer of step one of S3. In contrast, there is a charge transfer transition from HOMO localized on PIOG to LUMO which localized on RBeng. Fig. 10 shows the molecular orbitals involved in the electronic transitions of the molecules.

The HOMO and LUMO of product two are localized between two interacted molecules. This may interpret the difference behavior between the UV–vis spectra of the product and RBeng (Fig 3). The compound S4 showed highest energy gap (ΔE$_{gap}$ = 7.32 eV); which indicates its higher stability and less reactivity. The molecules that have the lowest energy gap are the molecule S3, S1 and S2 (ΔE$_{gap}$ = 6.42, 6.24, 5.97 eV) indicating their gradient lowest stability and high reactivity. The two properties like I (potential ionization) and A (affinity) are so important. These two parameters are related to the one-electron orbital energies of the HOMO and LUMO respectively. The more I is lower, the molecule will be the better electron donor. The more A is larger the molecule will be the better electron acceptor, thus RBeng acts as electron donor and PIOG acts as electron acceptor.
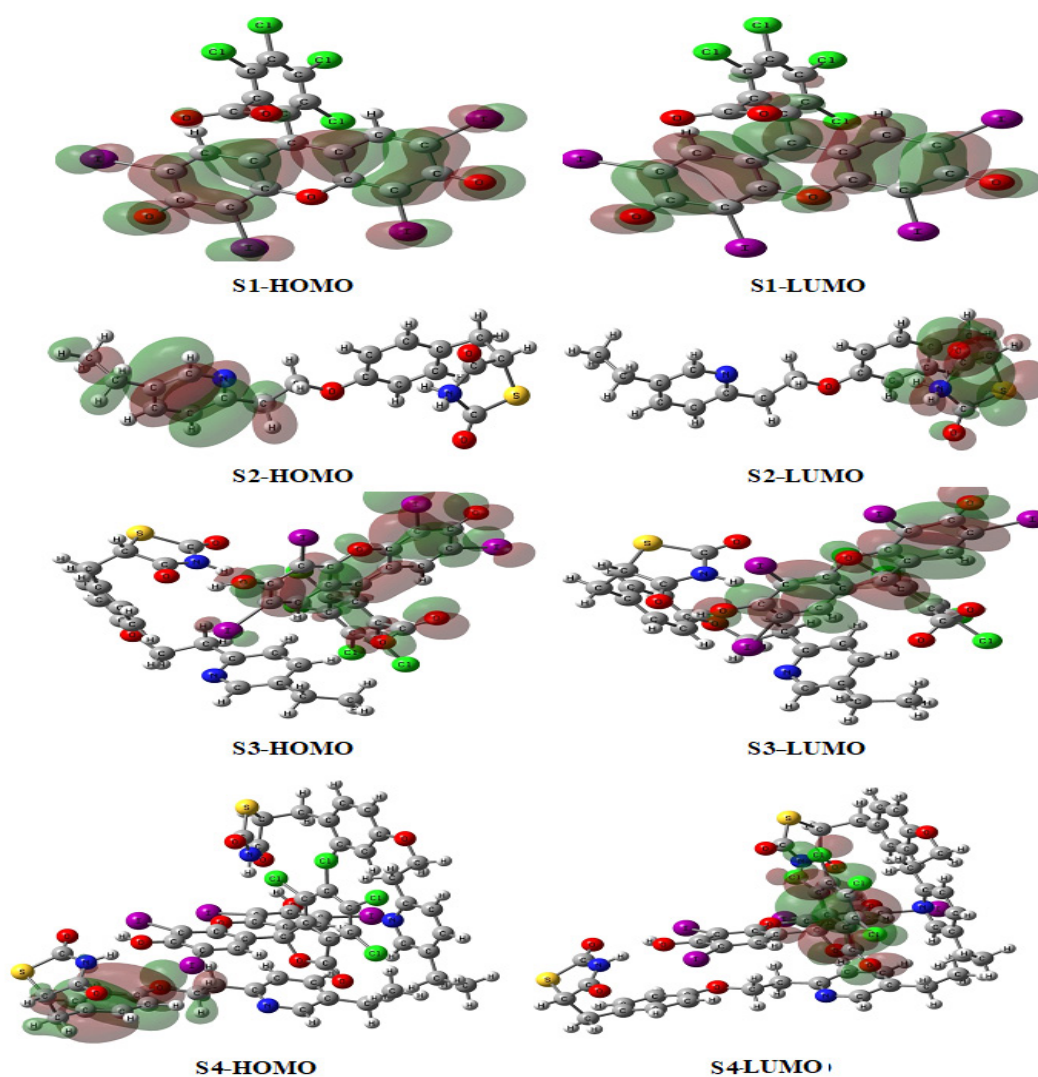
**Fig 10. HOMO and LUMO Frontier molecular orbitals of Compounds S1-S4.**

Energy gap ($\Delta E_{gap}$ (eV)) between HOMO and LUMO characterizes the molecular chemical stability which is a critical parameter in determining molecular electrical transport properties; because it is a measure of electron conductivity. The more negative value of energy gap in reagent (S1 = 6.24 eV) refers to chemical reactivity of this reagent to electrostatically attract to cationic drug (S2) of low value of energy gap (5.97eV). This interaction leads to the formation of proposed 1:1 (R:D) active product of high energy gap value (6.42 eV) and finally to the more stable separated solid product (1:2) of more energy gap (7.32 eV) than 1:1 but it is higher than that of reactants. This means that the 1:2 product is more reactive than corresponding reactants. This conclusion is also correlated to the HOMO and LOMO energy values; where HOMO energy characterizes the electron donating ability, while LUMO energy characterizes the electron withdrawing ability. In Table 7, the HOMO energy (eV) values of RBeng (S1 = -2.16), POIG drug (S2 = -10.71), R:D 1:1 product ( S3 = -5.75) and product 1:2 (S4 = -8.03); refer to the electron donating ability of rose bengal reagent to attract to the drug cation, and 1:1 product to attract to the second drug molecule to give 1: 2 product. The same order of donating power is also confirmed by LOMO energy values of RBeng (S1 = 3.81), POIG drug (S2 = -4.47), R:D 1:1 product (S3 = 0.67) and product 1:2 (S4 = -0.72) in which drug has the greatest electron attracting ability. This conclusion is also confirmed by theoretically calculated thermodynamic parameters (Table 8).

**TABLE 8. Theoretical thermodynamic parameters of PIOG (S1), RBeng (S2), RBeng-PIOG (S3,1:1) and RBeng-PIOG (1:2, S4).**

| Compound | E (Thermal) KCal/Mol | CV Cal/Mol-Kelvin | S Cal/Mol-Kelvin |
|---|---|---|---|
| PIOG Drug Cation (S1) | 247.565 | 89.303 | 174.338 |
| RBeng Reagent Anion (S2) | 124.769 | 106.744 | 218.409 |
| RBeng: Drug (1:1) (S3) | 402.634 | 186.200 | 331.933 |
| RBeng: Drug (1:2) (S4) | 639.429 | 285.421 | 440.959 |

The data in Table 8 refer to the stability order POIG (E = 247 K Cal mol$^{-1}$, CV = 89.303 Cal.mol K$^{o-1}$, S= 174.338 Cal. mol K$^{o-1}$) > RBeng(E = 124.769 K Cal mol$^{-1}$, CV = 106.744 Cal.mol K$^{o-1}$, S= 218.409 Cal.mol K$^{o-1}$)> product 1:2 (E = 639.42 K Cal mol$^{-1}$, CV = 285.421 Cal.mol K$^{o-1}$, S= 440.959Cal.mol K$^{o-1}$)> product 1:1(E = 402.634 K Cal mol$^{-1}$, CV = 186.200Cal.mol K$^{o-1}$, S= 331.933Cal.mol K$^{o-1}$). This means that the 1:1 product is less stable one and more reactive than 1:2 product.

*NBO atomic charges and MESP maps*

The NBO atomic charges and MESP maps are shown in Fig 11. The calculation of the NBO atomic charges has a very significant role in estimating the molecular properties and the reactivity of a molecule.

Fig. 11 shows that in PIOG drug S1; C41 has the largest positive charge (+0.75 e); which may be due to the electron withdrawing effect of the electronegative oxygen atom O42 of carbonyl group and nitrogen atom N40 of the thiazole ring and another high positive charge on H45 and H46 (0.53 and 0.51 e respectively). On the other hand, N40, C13, O42, and O43 atoms possess large negative charges (−0.8, -0.71, -0.42 and −0.46 e respectively).

Rbeng (S2) has the carbon atom C33 bears a positive charge of +0.793 e. The charges on the two oxygen atoms attached to C33 are all negative resulting in a net charge on the COO⁻ group of about −0.68 e and another negative sites O8 and O21 have -0.67 e. From the above results, it is clear that PIOG has several electrophilic sites; which can be easily attacked by one of the RBeng most nucleophilic sites (carboxylic group) with side oxygen. However, some of these interaction sites may not be feasible due to steric hindrance present in two RBeng molecules during their interaction with PIOG drug cation to form 1:2 (S4) product.

The MEPS analysis graphical representations are shown in Fig 12.

MESP analysis with the help of quantum mechanical methods has been used extensively to explain the reactive sites within compounds (S1-S4). MESP is found to be a useful descriptor

to predict reactive sites for electrophilic and nucleophilic attack reactions as well as hydrogen-bonding interactions [29]. In addition, they play a necessary role in the prediction of the molecular sites at which they are most likely to react [20]. MESP map of PIOG (S1), Fig. 12(a), indicates that; the electrostatic potential energy is maximum (electrophilic sites) at the quaternary ammonium salt group as indicated by the deep blue color. On the other hand, the MESP map of RBeng (S2) indicates that; the electrostatic potential energy is minimum (nucleophilic sites) at the carboxylic acid group with side two oxygen atoms as indicated by the deep red color, Fig. 12(b).

From the calculated atomic charges and MESP maps of the two molecules (S1 and S2) it is clear that; the interaction is preferred between O8, O21, O34, O35 of RBeng (S2) and C41, H45, H46 of PIOG (S1) molecule to form several kinds of H-bonds. The optimized geometry of the products S3 and S4is shown in Fig. 13.

These results show a complex structures of both products (S3 and S4); in which H36 is midway between O44 and O8 which indicates the formation of H–bond between the two molecules. Similarly, H40, H74 and H81 are midway between N37, C78, C70 and O8, O35, O35 respectively. Moreover, H62 and H63 form two H–bond between C60 and N67. Therefore, in case of S3 six hydrogen bonds (Table 9) were formed between the two molecules after protonation of PIOG and anion of RBeng (proton–transfer). Table 9 shows selected bond lengths and bond angles of the formed hydrogen bonds in the resulting PIOG-RBeng (1:1 product S3) which give binding energy of -185.59 kcal /mol.
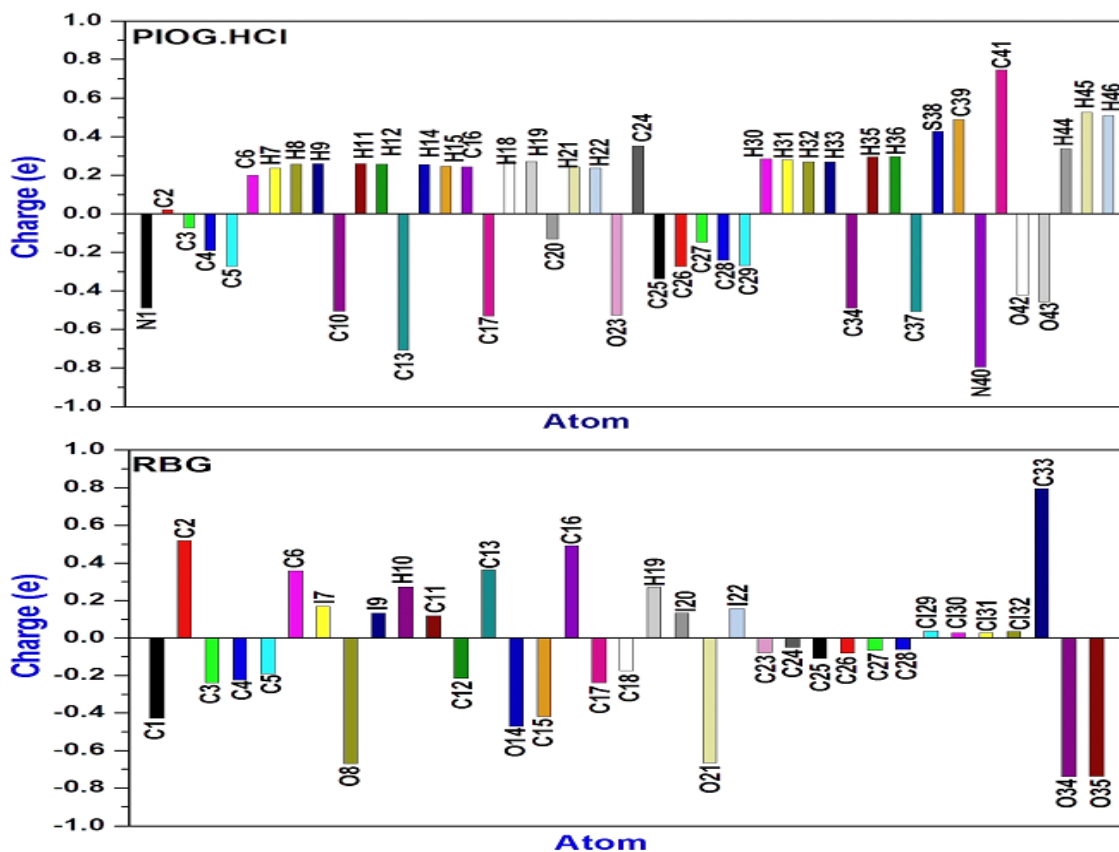
Fig. 11. NBO atomic charges of the studied molecules.
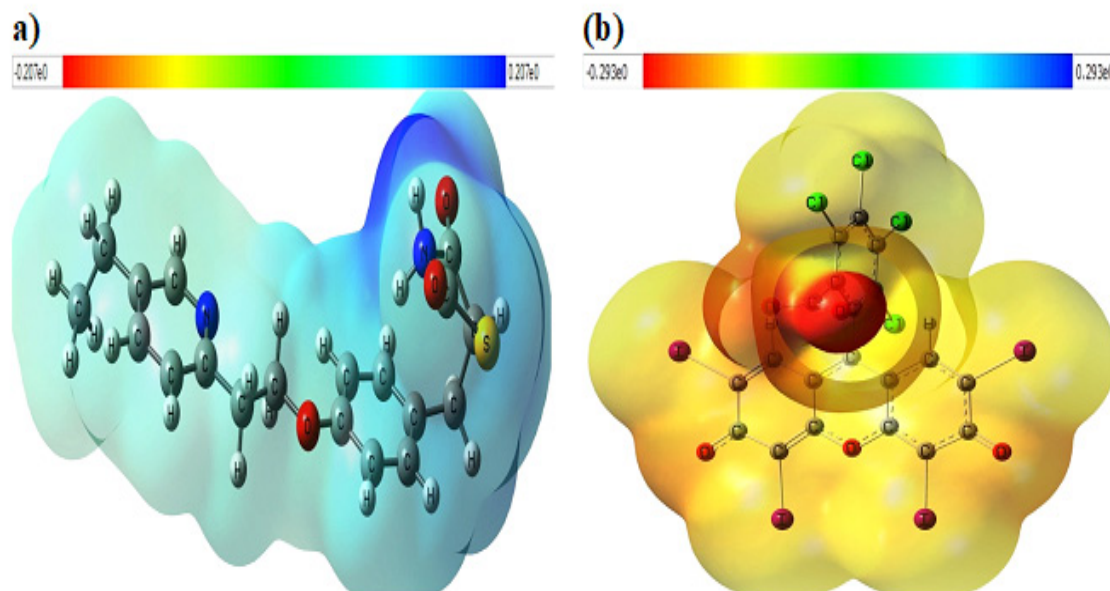


Fig. 12. MESP maps of the studied molecules showing the possible sites of interaction of PIOG.HCl (a) and RBeng (b).
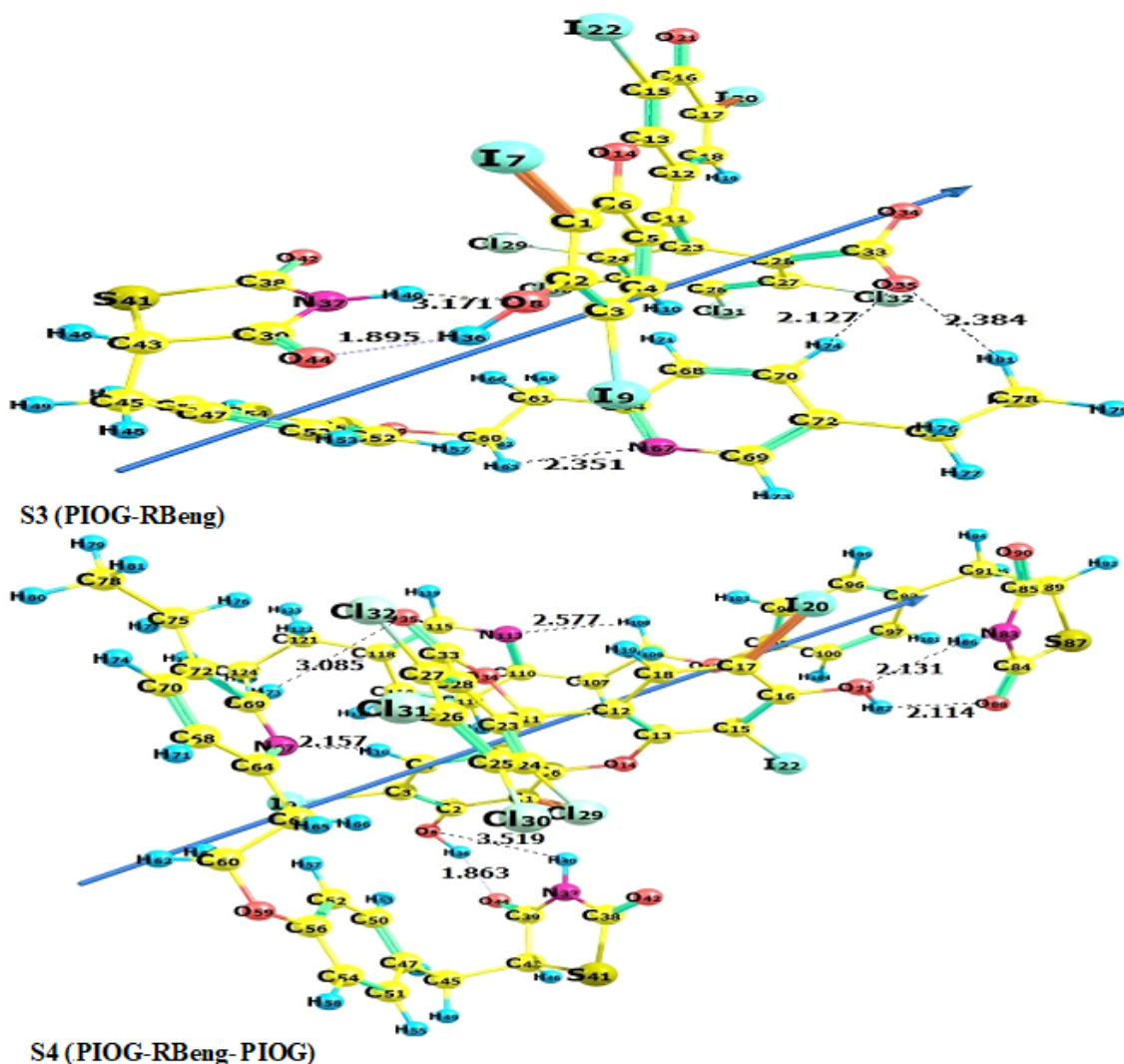
**Fig. 13. The optimized geometry, numbering system, vector of dipole moment of PIOG-RBeng (S3), and PIOG-RBeng-PIOG (S4) compounds with hydrogen bond interaction using WB97XD/GENECP level of calculation.**

**TABLE 9. Selected bond lengths showing the length of the formed six hydrogen bonds in PIOG-RBeng compound.**

| Bond | X–H...Y (Å) | Bond angles (°) |
|------|-------------|-----------------|
| O8–H36...O44 | 1.9 | 146.23 |
| N37–H40...O8 | 3.17 | 110.68 |
| C60–H62...N67 | 3.33 | 53.49 |
| C60–H63...N67 | 2.35 | 104.13 |
| C78–H74...O35 | 2.13 | 161.33 |
| C70–H81...O35 | 2.38 | 158.2 |

Whereas in case of PIOG-RBeng-PIOG product (1:2, S4) fifteen hydrogen bonds are formed (Table 10); as a result of reaction between one molecule of RBeng and two molecules of PIOG leading to a stable S4 product with binding energy of -353.03 kcal/mol. These results refer to high stability of S4 (1:2) product than S3 (1:1) product; which confirm previous practical conclusion.

*Local reactivity descriptor*

The concepts of local and global reactivity descriptors have been widely used to understand the chemical reactivity and site selectivity [59, 60]. To analyze molecular site selectivity, Parr and Yang [61] define local descriptors such as Fukui functions. Thus, calculating Fukui functions can enable us to determine the active sites of a molecule, based on the electronic density changes experienced by the molecule during a reaction. Fukui functions $f^+$(r), $f^-$(r) and $f^0$(r) are calculated for three chemical situations, using the following equations as [62]:

$f^- (r) = q_k(N) - q_k(N-1) \approx \rho^{HOMO}(r)$  forelectrophilic attack

$f^+ (r) = q_k(N+1) - q_k(N) \approx \rho^{LUMO}(r)$  fonucleophilic attack

$f^0 (r) = 1/2 [q_k(N+1) - q_k(N-1)] \approx 1/2[\rho^{HOMO}(r) + \rho^{LUMO}(r)]$  for Radical attack

Where is the atomic population on the $k_{th}$ atom for the neutral molecule, while and are the atomic population on the $k_{th}$ atom for its anionic and cationic species, respectively. In addition to the information concerning electrophilic and nucleophilic capacity of a given atomic site in the molecule, Labbe et al. [63] proposed another Dual descriptor which is given by:

$$\Delta f(r) = f^+ (r) - f^- (r)$$

Where is defined as the difference between the nucleophilic and electrophilic Fukui function. There are two situations need to be considered: if, then the site is favored for a nucleophilic attack, whereas if , then the site may be favored for an electrophilic attack. The calculation of Fukui functions indices and Dual descriptor of the interacted molecules obtained at the level WB97XD/GENECP level of theory is given in **Table 11**.

From the values of Fukui functions in the gas phase, it can be stated that; in PIOG (S1) molecule the most electrophilic active site is located on C2, C3, C5 and C6. Likewise, the active sites

susceptible for nucleophilic attacks are C37, S38, C41 and O42. In case Rbeng (S2), the most electrophilic active site is localized on C5, O8, C12 and C21. Likewise, the nucleophilic attacks active sites C11. The nature active sites change in case PIOG-RBeng (S3) with new sites but O8, O21 and carboxylic group are still prefer electrophilic attack with no effect of the PIOG nature; which prove the ion-pair mechanism with no charge transfer occur between two interacted molecules. On contrast, the results in PIOG-RBeng-PIOG (S4) indicate charge transfer between interacted electron donor and electron acceptor molecules to form several H-bonds in stable final 1:2 product. The same conclusion can be reached considering the Dual descriptor regarding both electrophilic and nucleophilic attack. This discussion had been previously concluded from NBO with MESP maps analyses [64, 65].

*Cytotoxicity*

The cytotoxic activities of PIOG (S1), RBeng (S2) and PIOG-RBeng product (S4) were studied against Caco-2 and Mcf7 cell lines. The results are shown in Fig. 14 and Table 12.

From Fig.11 it is obvious that; the viability of the Caco-2 and Mcf7 cell lines decreased by increasing the dose. PIOG (S1), RBeng (S2) and PIOG-RBeng product (S4) exhibited toxicity against Caco-2 with $IC_{50}$ values of 354.49, 422.22 and 402.66 μg/mL (Table 12), respectively. This means that 1:2 product S4 is the most effective against Caco-2 cells, where in case of Mcf7 cells with $IC_{50}$ values of 410.78, 346.39 and 785.34 μg/mL (Table 12), respectively; the most effective one is RBeng (S2) reagent.

Several cases of PIOG (S1)-induced liver injury have been reported [67, 68]. PIOG hepatotoxic effect has assessed on human HepG2 cells [69, 70]. In this study the hepatotoxicity of PIOG (S1), RBeng (S2) and PIOG-RBeng 1:2 product (S4) on human HepG2 cells was measured. From Fig. 12 (c), it's clear that at concentration range 125-500 μg/mL; PIOG-RBeng product was found non-toxic; while PIOG and RBeng showed toxicity to the cells (viability 29.97 % and 44.95% respectively) at this range. However, at concentration 1000 μg/mL the cell viability for PIOG-RBeng product was 86.39 % and for PIOG and RBeng was only 6.575 % and 20.34 % respectively. The cell viability decreased with increasing the concentration of the three samples.

**TABLE 10. Selected bond lengths showing the length of the formed fifteen hydrogen bonds PIOG-RBeng-PIOG compound.**

| Bond | X–H...Y (Å) | Bond angles (°) | Bond | X–H...Y (Å) | Bond angles (°) |
|---|---|---|---|---|---|
| O8–H36...O44 | 1.86 | 107.9 | N83–H86...O21 | 2.13 | 123.73 |
| N37–H40...O8 | 3.52 | 147.67 | C106–H8...N113 | 2.58 | 87.2 |
| C60–H62...N67 | 3.77 | 55.79 | C106–H109...N113 | 2.82 | 74.92 |
| C60–H63...N67 | 3.1 | 70.55 | C33–O35...H119 | 2.66 | 110.63 |
| C4–H10...N67 | 2.16 | 160.69 | C33–O35... 122 | 3.08 | 114.83 |
| C69–H73...O35 | 3.08 | 96.91 | C33–O34...H119 | 3.48 | 87.06 |
| C75–H76...O35 | 2.6 | 142.96 | C33–O34...H122 | 3.63 | 66.74 |
| O21–H82...O88 | 2.11 | 123.73 | | | |

**TABLE 11. Values of the Fukui functions and Dual descriptor of compounds S1-S4 at WB97XD/GENECP level of calculation .**

| | PIOG (S1) | | | | Rbengal (S2) | | | | Product 1:1 (S3) | | | Product 1:2 (S4) | | |
|---|---|---|---|---|---|---|---|---|---|---|---|---|---|---|
| Atoms | f(-) | f(+) | Δf | Atoms | f(-) | f(+) | Δf | f(-) | f(+) | Δf | f(-) | f(+) | Δf |
| N1 | 0.014 | 0.000 | -0.014 | C1 | 0.084 | 0.001 | -0.083 | 0.001 | 0.015 | 0.014 | 0.000 | 0.006 | 0.006 |
| C2 | **0.209** | 0.000 | **-0.209** | C2 | 0.022 | 0.060 | 0.037 | 0.038 | 0.069 | 0.032 | 0.000 | 0.010 | 0.010 |
| C3 | **0.260** | 0.000 | **-0.260** | C3 | 0.080 | 0.047 | -0.033 | 0.029 | 0.003 | -0.025 | 0.000 | -0.003 | -0.003 |
| C4 | 0.019 | 0.000 | -0.018 | C4 | 0.005 | **0.093** | **0.088** | 0.009 | **0.110** | **0.101** | 0.000 | -0.001 | -0.001 |
| C5 | **0.147** | 0.000 | **-0.147** | C5 | **0.144** | 0.025 | **-0.120** | **0.065** | 0.004 | **-0.062** | -0.001 | 0.014 | 0.015 |
| C6 | **0.225** | 0.001 | **-0.224** | C6 | 0.006 | 0.057 | 0.051 | 0.030 | 0.044 | 0.014 | 0.000 | -0.007 | -0.007 |
| H8 | 0.000 | 0.000 | 0.000 | O8 | **0.106** | 0.054 | **-0.052** | 0.018 | 0.012 | -0.006 | 0.000 | 0.000 | 0.000 |
| H11 | 0.011 | 0.000 | -0.011 | C11 | 0.004 | **0.288** | **0.283** | 0.071 | **0.235** | **0.164** | 0.000 | -0.022 | -0.021 |
| H12 | 0.002 | 0.000 | -0.002 | C12 | **0.142** | 0.026 | **-0.116** | 0.080 | **0.094** | **0.014** | 0.001 | 0.007 | 0.006 |
| C13 | 0.034 | 0.000 | -0.034 | C13 | 0.006 | 0.058 | 0.052 | 0.020 | 0.063 | 0.042 | -0.004 | -0.001 | 0.003 |
| H15 | 0.001 | 0.000 | -0.001 | C15 | 0.082 | 0.002 | -0.080 | **0.140** | 0.020 | **-0.121** | -0.013 | -0.006 | 0.008 |
| H18 | 0.015 | 0.000 | -0.015 | C18 | 0.005 | 0.090 | 0.085 | 0.003 | 0.068 | 0.066 | -0.002 | -0.003 | -0.002 |
| H21 | 0.001 | 0.000 | -0.001 | O21 | **0.103** | 0.056 | **-0.047** | **0.082** | 0.079 | **-0.004** | 0.001 | 0.000 | -0.001 |
| H22 | 0.001 | 0.000 | -0.001 | I22 | 0.027 | 0.001 | -0.026 | **0.116** | 0.002 | **-0.114** | 0.002 | 0.001 | 0.000 |
| O23 | 0.001 | -0.001 | -0.002 | C23 | 0.000 | 0.035 | 0.035 | -0.004 | 0.020 | 0.024 | 0.000 | 0.085 | 0.086 |
| C25 | 0.001 | -0.031 | -0.032 | C25 | 0.000 | -0.044 | -0.044 | 0.004 | -0.013 | -0.017 | 0.000 | **0.211** | **0.212** |
| C27 | 0.001 | -0.051 | -0.052 | C27 | 0.000 | -0.004 | -0.004 | 0.000 | -0.009 | -0.009 | 0.000 | **0.124** | **0.124** |
| C28 | 0.000 | 0.049 | 0.049 | C28 | 0.000 | -0.021 | -0.021 | 0.014 | -0.005 | -0.019 | 0.000 | **0.226** | **0.226** |
| H33 | 0.000 | 0.000 | 0.000 | C33 | 0.002 | -0.007 | -0.009 | -0.003 | -0.002 | 0.000 | 0.000 | **0.086** | **0.086** |
| C34 | 0.000 | 0.005 | 0.005 | O34 | 0.004 | 0.000 | -0.004 | **0.108** | 0.001 | **-0.108** | 0.000 | **0.029** | **0.029** |
| H36 | 0.000 | 0.012 | 0.012 | O35 | 0.005 | 0.001 | -0.004 | 0.050 | 0.001 | -0.050 | 0.000 | **0.080** | **0.080** |
| C37 | 0.000 | **0.093** | **0.093** | N37 | | | | 0.001 | 0.004 | 0.003 | 0.000 | 0.000 | 0.000 |
| S38 | 0.000 | **0.105** | **0.105** | C38 | | | | 0.000 | -0.004 | -0.005 | 0.000 | -0.001 | -0.001 |
| C39 | 0.000 | 0.031 | 0.031 | S41 | | | | 0.000 | 0.000 | 0.000 | 0.000 | 0.000 | 0.000 |
| N40 | 0.000 | 0.031 | 0.031 | O42 | | | | 0.000 | 0.000 | 0.000 | 0.000 | 0.000 | 0.000 |
| C41 | 0.000 | **0.427** | **0.427** | C93 | | | | | | | **0.242** | 0.000 | **-0.242** |
| O42 | 0.000 | **0.258** | **0.258** | C96 | | | | | | | 0.056 | 0.001 | -0.055 |
| O43 | 0.000 | 0.014 | 0.014 | C98 | | | | | | | **0.099** | 0.001 | **-0.098** |
| H44 | 0.000 | 0.009 | 0.009 | C100 | | | | | | | **0.130** | 0.000 | **-0.130** |
| H45 | 0.000 | 0.025 | 0.025 | C102 | | | | | | | **0.173** | -0.001 | **-0.174** |
| H46 | 0.000 | 0.018 | 0.018 | O105 | | | | | | | **0.196** | 0.000 | **-0.196** |
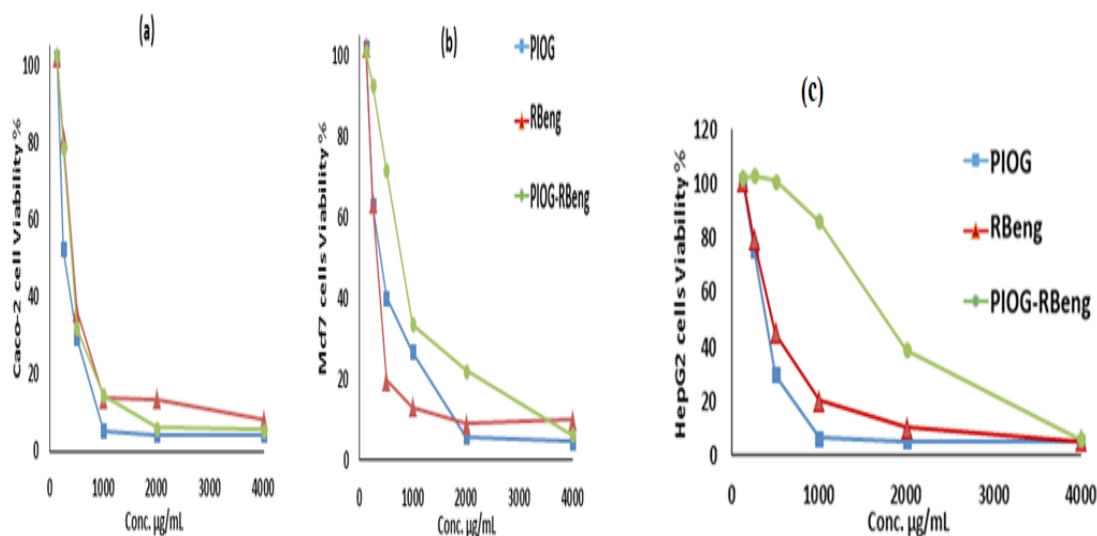
**Fig. 14. Cytotoxicity of PIOG (S1), RBeng (S2) and PIOG-RBeng (S4) against (a) Caco-2 cells    (b) Mcf7 cells and (c) HepG2 cells.**

**TABLE 12. Cytotoxicity effect (IC$_{50}$ µg/mL) of PIOG, RBeng and their product against Caco-2, Mcf7 and HepG2 cell lines.**

| Sample | IC$_{50}$ µg/mL | | |
| --- | --- | --- | --- |
| | Caco-2 | Mcf7 | HepG2 |
| **PIOG** | 354.49 | 410.78 | 392.01 |
| **RBeng** | 422.22 | 346.39 | 597.74 |
| **PIOG-RBeng** | 402.66 | 785.34 | 2175.4 |

From Table 12, also the IC$_{50}$ of PIOG (S1) and RBeng (S2) for human HepG2 cells were 392.01 and 597.74 µg/mL respectively; while for PIOG-RBeng 1: 2 product (S4) it was 2175.4 µg / mL. Form these results, it's obvious that PIOG-RBeng S4 product showed less hepatotoxicity than S1 and S2 and consequently it has less anticancer activity for HepG2 cells. This may be attributed to masking of active functional groups of RBeng by electrostatic attraction and hydrogen bonding with the groups of two PIOG drug in S4 1:2 product.

**References**

1.  O'Neil M.J., Heckelman P.E., Koch C.B. and Roman K.J., The Merck Index. 14th ed., Merck & Co. Inc.; Whitehouse Station, NJ: 1284 (2006).

2.  [Online] available: http://www.accessdata.fda. gov/drugsatfda_docs/label/2013/021073s046lbl. pdf

3.  Ho E.N.M., Yiua K.C.H., Wana T.S.M., Stewartb B.D. and Watkins K.L., Detection of anti-diabetics in equine plasma and urine by liquid chromatography-tandem mass spectrometry. J Chromatogr B Analyt Technol Biomed Life Sci, 811, 65–73 (2004).

4.  Lin Z.J., Ji W., Krieger D.D.– and Shum L., Simultaneous determination of pioglitazone and its two active metabolites in human plasma by

LC–MS/MS. J Pharm Biomed Anal, 33, 101–108 (2003).

5. Karra V.K., Pilli N.R., Inamadugu J.K. and Rao J.V.L.N.S., Simultaneous determination of pioglitazone and candesartan in human plasma by LC-MS/MS and its application to a human pharmacokinetic study. J Pharm Anal, 2, 167–173 (2012).

6. Singh S.C.D.D. and Kushnoor A., Development and validation of a HPTLC method for estimation of pioglitazone in bulk and tablet dosage form. J Pharm Res, 4, 3919–3921 (2011).

7. Anand D.P., Senthilkumar K.L., Senthilkumar B., Saravanakumar M. and Thirumurthy R., HPTLC method for determination of telmesartan HCl with pioglitazone HCl in pharmaceutical dosage form. Int J Pharm Res, 2, 185–190 (2010).

8. Sharma M., Sharma S. and Kohli D., HPTLC method development and validation for the estimation of atorvastatin calcium and pioglitazone HCl in pharmaceutical combined tablet dosage form. Ann Biol Res, 1, 124–129 (2010).

9. Amanlou M., -Ghobadi M.Z., Rofouei M.K., Saremi S. and Kebriaeezadeh A., Extractive spectrophotometric method for determination of pioglitazone HCl in raw material and tablets using ion-pair formation. J Chem, 7, 915–921 (2010).

10. Okdeh M., Sakur A.A. and Alfares B., Determination of pioglitazone in bulk and pharmaceutical formulations by extractive spectrophotometric method using ion – pair formation. Int J Pharm Pharm Sci, 6, 43–47 (2014).

11. Adhikari L., Jagadev S., Sahoo S., Murthy P.N. and Mishra U.S., Devlopement and validation of UV-visible spectrophotometric method for simultaneous determination of pioglitazone hydrochloride, metformin hydrochloride and glipizide in its bulk and pharmaceutical dosage form (tablet). Int J Chem Tech Res, 4, 625–630 (2012).

12. Game M.D., First order derivative spectrophotometric method for simultaneous estimation of glimepiride and pioglitazone HCl in combined dosage form. J Pharm Res, 4, 4301–4302 (2011).

13. Kishore L. and Kaur N., Estimation of pioglitazone and glimipride in its pharmaceutical dosage form by spectrophotometric methods. Der Pharm Lett, 3, 276–284 (2011).

14. Mohd S., Kulkarni A.P. and Zaheer Z., Spectroscopic estimation of pioglitazone hydrochloride. Int J Pharm Frontier Res, 2, 87–94 (2012).

15. Patil S., Dwivedi S. and Bagade S., Development of spectrophotometric method for the estimation of pioglitazone HCl from two different marketed brands. Am J Pharm Tech Res, 1, 264–275 (2011).

16. Parham H., Zargar B., Heidari Z. and Hatamie A., Magnetic solid-phase extraction of rose bengal using iron oxide nanoparticles modified with cetyltrimethylammonium bromide. J Iran Chem Soc, 8, S9–S16 (2011).

17. Mousavi S.H., Afshari J.T., Brook A. and Anarkooli I.J., Direct toxicity of rose bengal in MCF-7 cell line: role of apoptosis. Food Chem Toxicol, 47, 855–859 (2009).

18. Xu D. and Neckers D.C., Aggregation of rose bengal molecules in solution. J PhotochPhotobio A: Chem, 40, 361–370 (1987).

19. Ito T. and Kobayashi K., A survey of in vivo photodynamic activity of xanthenes, thiazines, and acridines in yeast cells. Photochem Photobiol, 26, 581–587 (1997).

20. Theodossiou T., Hothersall J.S., Woods E.A., Okkenhaug K., Jacobson J. and MacRobert A.J., Firefly luciferin-activated rose bengal: in vitro photodynamic therapy by intracellular chemiluminescence in transgenic NIH 3T3 cells. Cancer Res, 15, 1818–1821 (2003).

21. Delprat G.D., Epstein N.N. and Kerr W.J., A new liver function test: the elimination of rose bengal when injected into the circulation of human subjects. Arch Intern Med, 34, 533–541 (1924).

22. Nordyke R.A., Surgical vs. nonsurgical jaundice: differentiation by a combination of rose bengal i131 and standard liver-function tests. JAMA, 194, 949–953 (1965).

23. Argueso P., Tisdale A., Michaud S.S., Sumiyoshi M. and Gipson I.K., Mucin characteristics of human corneal-limbal epithelial cells that exclude the rose bengal anionic dye. Invest Ophthalmol Vis Sci, 47, 113–119 (2006).

24. Wachter E., Dees C., Harkins J., Scott T., Petersen M. and Rush R.E., Amy Cada; Topical Rose Bengal: pre-clinical evaluation of pharmacokinetics and safety. Lasers Surg Med, 32, 101–110 (2003).

25. Chang C.C., Yang Y.T., Yang J.C., Wu H.D. and Tsai T., Absorption and emission spectral shifts of rose bengal associated with DMPC liposomes. Dyes Pigm, 79, 170–175 (2008).

26. Carreon J.R., Roberts M.A., Wittenhagen L.M. and Kelley S.O., Synthesis, characterization, and cellular uptake of DNA-binding rose bengal peptidoconjugates., Org Lett, 7, 99–102 (2005).

27. Mousavi S.H., Zhang X.D., Sharifi A.M. and Hersey P., Study of rose bengal-induced cell death in melanoma cells in the absence of light. Iran J Basic Med Sci, 9, 216–222 (2006).

28. Lee J.S., Lee B.I. and Park C.B., Photo-induced inhibition of Alzheimer's β-amyloid aggregation in vitro by rose bengal. Biomaterials, 38, 43–49 (2015).

29. Frisch M.J., Trucks G.W., Schlegel H.B., Scuseria G.E., Robb M.A., Cheeseman J.R., et al., Gaussian Inc., Wallingford, CT (2010).

30. Becke A.D., Phys Rev A, 38, 3098 (1988).

31. Becke A.D., J Chem Phys, 98, 5648 (1993).

32. Johnson B.G. and Frisch M.J., Chem Phys Lett, 216, 133 (1993).

33. Lee C., Yang W. and R. G., Phys Rev B, 37, 785 (1988).

34. Weigend F. and Ahlrichs R., Phys Chem Chem Phys, 7, 3297 (2005).

35. Schafer A., Huber C. and Ahlrichs R., J Chem Phys,100, 5829 (1994).

36. McLean A.D. and Chandler G.S., J Chem Phys, 72, 5639 (1980).

37. Ditchfield R., Hehre W.J. and Pople J.A., J Chem Phys, 54 (2), 724 (1971).

38. Ulic S.E., Vedova C.O.D., Hermann A., Mack H.G. and Oberhammer H., J Phys Chem A, 112, 6211 (2008).

39. Reed A.E. and Weinhold F., Chem J Phys,78, 4066 (1983).

40. Xuefei X. u.D.G., J Chem Theory Comput, 7, 2766 (2011).

41. R. G., Proc Natl Acad Sci, 83, 8440 (1986).

42. Chandra A.K. and Uchimara T., J Phys Chem A, 105, 3578 (2001).

43. Calu L., Badea M., Chifiriuc M.C., Bleotu C., Iulia David G., Ionita G., et al., J Therm Anal Calorim, 120, 375 (2015).

44. Bauernschmitt R. and Ahlrichs R., Chem Phys Lett; 256, 454–464 (1996).

45. Casida M.E., Jamorski C., Casida K.C. and Salahub D.R., J Chem Phys, 108, 4439 (1998).

46. Stratmann R.E., Scuseria G.E. and Frisch M.J., J Chem Phys, 109 , 8218 (1998).

47. Caillie C.V. and R. D., Chem Phys Lett, 308, 249 (1999).

48. Caillie C.V. and Amos R.D., Chem Phys Lett, 317, 159 (2000).

49. Furche F. and Ahlrichs R., J Chem Phys, 117, 7433 (2002).

50. Scalmani G., Frisch M.J., Mennucci B., Tomasi J., Cammi R. and Barone V., J Chem Phys, 24, 1 (2006).

51. Kumasaki M., Sasahara K. and Nakajima Y., Therm Anal Calorim, 125, 331 (2016).

52. Avci D., Basoglu A. and Atalay Y., Struct Chem, 21, 213 (2010).

53. Avci D., Comert H. and Atalay Y., J Mol Model, 14, 161(2008).

54. Bauer A.W., Kirby W.M., Sherris C. and Turck M., Antibiotic susceptibility testing by a stnadardized single disk method. Am J Clin Pathol, 45, 493–496 (1966).

55. Pfaller M.A., Burmeister M.A. and Bartlett M.G. Multicenter evaluation of four methods of yeast inoculum preparation. J Clin Microbiol, 26, 1437–1441 (1988).

56. National Committee for Clinical Laboratory Standards, Performance. Vol 41, 1997 Antimicrobial Susceptibility of Flavobacteria (1993).

57. Socrates G., Infrared and Raman Characteristic Group Frequencies: Tables and Charts, John Wiley & Sons: 18 (2004).

58. Gadape H. H. and Parikh K. S., Quantitative determination and Validation of Pioglitazone in Pharmaceutical using Quantitative Nuclear Magnetic Resonance Spectroscopy. J. Chem. Pharm. Res, 3(1): 649-664 (2011).

59. Morris G.M. and Goodsell D.S., Automated docking using a Lamarckian genetic algorithm

and an empirical binding free energy function. J Comput Chem, 19, 1639–1662 (1998).

60. Chai J.D. and Head-Gordon M., Long-range corrected hybrid density functionals with damped atom-atom dispersion corrections. Phys Chem Chem Phys, 10, 6615–6620 (2008).

61. Weigend F. and Ahlrichs R., Phys Chem Chem Phys, 7, 3297 (2005).

62. Xu X. and Truhlar D.G., J Chem Theory Comput, 7, 2766–2779 (2011).

63. http://www.chemcraftprog.com.GaussView, Version 5, R. Dennington, T. Keith, J. Millam, Semichem Inc., Shawnee Mission KS (2009).

64. Zayed M.A. and Eladly A.A., The use of two novel maleanilinic acid indicators in ground water analyses applying UV-vis spectra and atomic spectrometry and biological studies of these derivatives. Egypt J Chem, 62, 157–170 (2019).

65. Zayed M.A., El-Desawy M. and Eladly A.A.. Spectroscopic investigation of para-methyl and para-methoxy maleanilic acids in comparison with thermal analyses and theoretical calculations. Egypt J Chem, 62, 1519–1536 (2019).

66. Marcy T. R., Britton M. L., Blevins S. M., Second Generation Thiazolidinediones and

67. Hepatotoxicity. Ann Pharmacother, 38, 1419-1423 (2004).

68. May L. D., Lefkowitch J. H., Kram M. T., Rubin D. E., Mixed Hepatocellular–Cholestatic Liver Injury After Pioglitazone Therapy. Ann Intern Med, 136, 449-452 (2002).

69. Liu H., Zhang C., Song F., Xiao T., Meng J., Zhang Q., Liang C., Li S., Wang J., Zhang B., Liu Y., Sun T., and Zhou H., A Novel Partial Agonist of Peroxisome Proliferator-Activated Receptor g with Excellent Effect on Insulin Resistance and Type 2 Diabetes. J Pharmacol Exp Ther, 353, 573–581, (2015).

70. Niknahad H., Heidari R., Alzuhairi A. M., Najibi A., Mitochondrial Dysfunction as a Mechanism for Pioglitazone-Induced Injury toward HepG2 Cell Line. Pharma Sci, 20, 169-174 (2015).

دراسة تركيب ناتج تفاعل كاشف الروزبنجال مع دواء البيجليتازون الجديد وخواصة في معالجة الخلايا السرطانية وتقيم تلك الدراسة ومقارنتها بالحسابات النظرية

محمد عبد الجواد زايد¹، ياسمين سعد فراج¹، محمود أحمد نعمان²

¹قسم الكيمياء ـ كلية العلوم ـ جامعة القاهرة ـ الجيزه ـ مصر.

²قسم الرياضيات ـ كلية العلوم ـ جامعة القاهرة ـ الجيزه ـ مصر.

في هذا البحث تم تحضيرودراسة تركيب نواتج تفاعل كاشف الروزبنجال مع دواء البيجليتازون الجديدة بواسطة التحليل العنصري الميكروني والتحليل الحراري والطيف في مدي الأشعة تحت الحمراء والرنين النووي المعناطيسي للبروتون وأشعة أكس. وتم دعم تلك النتائج بالحسابات النظرية والتي اكدت تراكيب تلك المواد في الصيغة العامة والصيغ البنائية وتحديد المجموعات النشطة بها. كما اكدت خط سير تلك التفاعلات حتي الوصول الي النواتج النهائية. وتمت تلك الحسابات النظرية بواسطة برنامج الجاويسين مع حساب كل الدوال والعوامل المؤثرة في تلك الحسابات مع أستخدام أحدث النظريات الحسابية. كما تم دراسة استخدام تلك النواتج الجديدة في مقاومة الخلايا السرطانية للقولون والصدروالتي ثبت فعاليتها لمقاومة تلك الخلايا مقارنة بالمواد القياسية المستخدمة في هذا المجال.